

A Regression-Based Approach to the CO₂ Airborne Fraction: Enhancing Statistical Precision and Tackling Zero Emissions

Mikkel Bennedsen, Eric Hillebrand, Siem Jan Koopman

August 22, 2024

Abstract

The global fraction of anthropogenically emitted carbon dioxide (CO₂) that stays in the atmosphere, the CO₂ airborne fraction, has been fluctuating around a constant value over the period 1959 to 2022. The consensus estimate of the airborne fraction is around 44%; the remaining 56% is absorbed by the oceanic and terrestrials biospheres. In this study, we show that the conventional estimator of the airborne fraction, based on a ratio of changes in atmospheric CO₂ concentrations and CO₂ emissions, suffers from a number of statistical deficiencies, such as non-existence of moments and a non-Gaussian limiting distribution. We propose an alternative regression-based estimator of the airborne fraction that does not suffer from these deficiencies. We show that the regression-based estimator has a Gaussian limiting distribution and reduces estimation uncertainty substantially. Our empirical analysis leads to an estimate of the airborne fraction over 1959–2022 of 47.0% ($\pm 1.1\%$; 1σ), implying a higher, and better constrained, estimate than the current consensus. Using climate model output, we show that a regression-based approach provides sensible estimates of the airborne fraction, also in future scenarios where emissions are at or near zero.

The amount of anthropogenically emitted carbon dioxide (CO₂) that stays in the atmosphere, the so-called *airborne fraction* (AF), is an important quantity for the study of CO₂ absorption in the carbon-cycle of the Earth system (Bacastow and Keeling, 1973; Siegenthaler and Oeschger, 1978; Gloor et al., 2010). In the literature it has been investigated and debated whether the AF has increased, decreased, or remained constant over the period from 1959 to today, during which atmospheric measurements of CO₂ concentrations have been available. Earlier studies found evidence of an increasing AF (e.g. Canadell et al., 2007; Raupach et al., 2008; Le Quéré et al., 2009), even though measurement and estimation uncertainty make these findings statistically dubious (e.g. Knorr, 2009; Ballantyne et al., 2015). Later studies suggest that the AF has remained constant around 44%, and this has become the consensus view (Raupach et al., 2014; Bennedsen et al., 2019; Canadell et al., 2021; Bennedsen et al., 2023b). Raupach (2013) shows that the AF is given by a constant in a system where emissions follow an exponential trajectory and the sink uptake is linear in atmospheric CO₂ concentrations. Bennedsen et al. (2023a) formalize such a system statistically, also allowing for linear growth of emissions on the more recent sample, and report a point estimate of the AF of 0.44.

Previous studies have analyzed the AF as the ratio of yearly changes in atmospheric CO₂ concentrations (G_t , numerator) and anthropogenic CO₂ emissions (E_t , denominator) (e.g. Canadell et al., 2007; Raupach et al., 2008; Le Quéré et al., 2009; Knorr, 2009; Ballantyne et al., 2012; Raupach et al., 2014; Ballantyne et al., 2015; Keenan et al., 2016; Bennedsen et al., 2019; van Marle et al., 2022; Pressburger et al., 2023). An alternative to this approach is to consider the *cumulative airborne fraction* (CAF; e.g., Jones et al., 2013, 2016; Liddicoat et al., 2021), but since this approach is less commonly used in the literature and is less amenable to statistical analysis, we only briefly address the CAF in our empirical applications and omit it from our theoretical discussions. Instead, we follow the main body of the literature and adopt the conventional estimator of the AF which is defined as the sample mean of the yearly ratio G_t/E_t . In this paper, we show that this estimator suffers from a number of statistical deficiencies due to its definition as the ratio of two stochastic processes. One problem is that the denominator in the ratio, E_t , may have a positive probability density at zero, implying that the estimator does not possess any moments. This lack of moments implies, for instance, that the mean and variance of the estimator do not exist. Although this issue may be of limited concern during the period 1959–2022, it becomes important in future scenarios where CO₂ emissions decrease, such as those consistent with “net-zero” CO₂ emissions, a committed goal of the international community (Rockström et al., 2017; Riahi et al., 2022). For example,

issues with the conventional analysis of the AF when emissions decrease are recently encountered in [Pressburger et al. \(2023\)](#), where the future AF implied by output from a climate model is studied. Another problem is that the time series of yearly changes in atmospheric concentrations G_t and emissions E_t exhibit a trend, which implies that a central limit theorem does not hold for the estimator. Therefore, its limiting distribution may be non-Gaussian, unless a separate assumption of Gaussianity is imposed. This implies that confidence intervals and p -values for test statistics based on the Gaussian distribution may not be valid for the conventional ratio-based estimator.

We show that the time series of yearly changes in atmospheric CO₂ concentrations, G_t , cointegrates with the time series of anthropogenic CO₂ emissions, E_t , over the period 1959–2022. Cointegration means that, even though G_t and E_t are non-stationary time series individually, the linear regression equation $G_t = \alpha E_t + u_t$, with constant parameter α , has a stationary error u_t . In other words, the non-stationary processes G_t and E_t are cointegrated when a linear combination exists that yields a stationary process. The parameter α denotes the fraction of emissions that is added to the atmosphere in year t , i.e., in the linear regression, α represents the AF. We show the constancy of α statistically on the historical sample. In future scenarios where emissions decrease substantially, α will be time-varying, however.

We show that estimating α using an ordinary least squares method applied to the linear regression equation $G_t = \alpha E_t + u_t$ yields an AF estimator with superior statistical properties compared to the conventional AF estimator based on the ratio G_t / E_t . This regression-based estimator does not suffer from the defects of the ratio-based estimator described above, and, under mild assumptions, converges to the true value α at the fast rate of $T^{3/2}$, where T is the sample size. A central limit theorem applies to the regression-based estimator, i.e. the estimator has a Gaussian distribution as the sample size increases to infinity for a wide range of distributions that can be assumed for the regression error u_t . Conventional confidence intervals and p -values for various test statistics based on the Gaussian distribution are therefore valid for the regression-based estimator. We generalize the regression approach such that α is time-varying for the study of future net-zero emission scenarios.

We apply the ratio-based and the regression-based estimators of the AF to yearly data from the Global Carbon Project ([Friedlingstein et al., 2023](#)) over the period 1959–2022, and we find that the regression-based estimator improves precision, as measured by the standard error of the estimator, by approximately 11% compared to the ratio-based estimator. Our estimate of the AF over the period 1959–2022 is 44.8% with an associated standard error of 1.4%. Hence, this estimate is not

significantly different from the consensus estimate of 44%. To further reduce estimation uncertainty, we also consider the inclusion of additional data on the El Niño-Southern Oscillation (ENSO) and volcanic activity as covariates in the analysis (Raupach et al., 2008). In this case, the regression-based estimator improves precision by approximately 16%, compared to the ratio-based estimator of the AF. Our best estimate of the AF over the period 1959–2022 is 47.0% with an associated standard error of 1.1%, which leads to a 95% confidence interval of [44.9%, 49.0%] for the AF. The consensus estimate of 44% (Canadell et al., 2021, p. 676) falls just outside this confidence interval. Our empirical results thus imply a higher, and better constrained, AF than the current consensus. The higher value of the estimate is mainly driven by the inclusion of ENSO and volcanic activity; the tighter confidence interval is mainly driven by the regression-based estimation approach.

We find that the AF has remained approximately constant over the historical period 1959–2022, corroborating earlier results (Raupach et al., 2014; Bennedsen et al., 2019; Canadell et al., 2021). Future trajectories of emissions will likely result in a non-constant AF, however. This may be either because of emissions trajectories departing from exponential growth or from changing dynamics in the carbon sinks, arising from e.g. saturation (Le Quéré et al., 2007; Canadell et al., 2007) or climate feedback effects (Friedlingstein, 2015), resulting in a non-linear relationship between sink activity and atmospheric concentrations. Climate models have shown that the AF tends to increase in future high-emission scenarios and decrease in low-emission scenarios (Jones et al., 2013). Using output from the reduced-complexity climate model MAGICC (Meinshausen et al., 2011), we illustrate the challenges in applying the ratio-based estimator of the AF to low-emission scenarios, and we show that a regression-based approach alleviates these difficulties. Furthermore, we show that generalizing the regression-based estimator to a time-varying AF can be a powerful tool in analyzing the dynamics of the AF in low-emission scenarios output from climate models, such as scenarios compatible with the Paris Agreement.

Atmospheric changes, emissions, and cointegration

Figures 1a) and 1b) show yearly changes in atmospheric CO₂ (G_t) and yearly CO₂ emissions from anthropogenic sources (E_t), respectively. The black line in Figure 1c) shows the ratio of these two variables, G_t/E_t . Data are obtained from the Global Carbon Project and cover the period 1959–2022; in the empirical section below we provide further details on the data. The most conspicuous feature of the two data series G_t and E_t is that both time series exhibit upwards

trends. Trending behavior is indicative of time series being non-stationary. A simple least-squares statistical analysis of the bivariate system (G_t, E_t) , where the non-stationarity of a time series is not accounted for, yields invalid inference and should be avoided (Granger and Newbold, 1974). However, the notion of cointegration (see, for example, chapter 19 in Hamilton, 1994, for a textbook treatment) allows us to keep working with the trending time series G_t and E_t while still obtaining valid statistical inference. Cointegration methods have been applied in earlier climate studies (e.g. Kaufmann and Stern, 2002; Schmith et al., 2012). Informally, two time series are cointegrated if they share a common trend. Formally, the time series G_t and E_t are said to be cointegrated when both G_t and E_t are non-stationary, and the error term u_t in the regression equation $G_t = \alpha E_t + u_t$ is stationary. We adopt the Dickey-Fuller test (Dickey and Fuller, 1979) to determine whether a time series is non-stationary. The test statistic is for the null hypothesis of a unit root, that is, of having a unit value for the autoregressive dependence of G_t on its lagged value G_{t-1} (and E_t on E_{t-1}). The results from this test strongly suggest that both time series are non-stationary (Supplementary Information S2.1). The null hypothesis of no cointegration (that is, u_t is non-stationary) can be tested formally using the Engle-Granger test (Engle and Granger, 1987), which is a Dickey-Fuller test on the residuals in the regression $G_t = \alpha E_t + u_t$, adjusted for the fact that these residuals are not observed but must be estimated. The null hypothesis of a unit root in u_t is firmly rejected (Supplementary Information S2.1), and we can therefore conclude that the two yearly time series G_t and E_t are cointegrated.

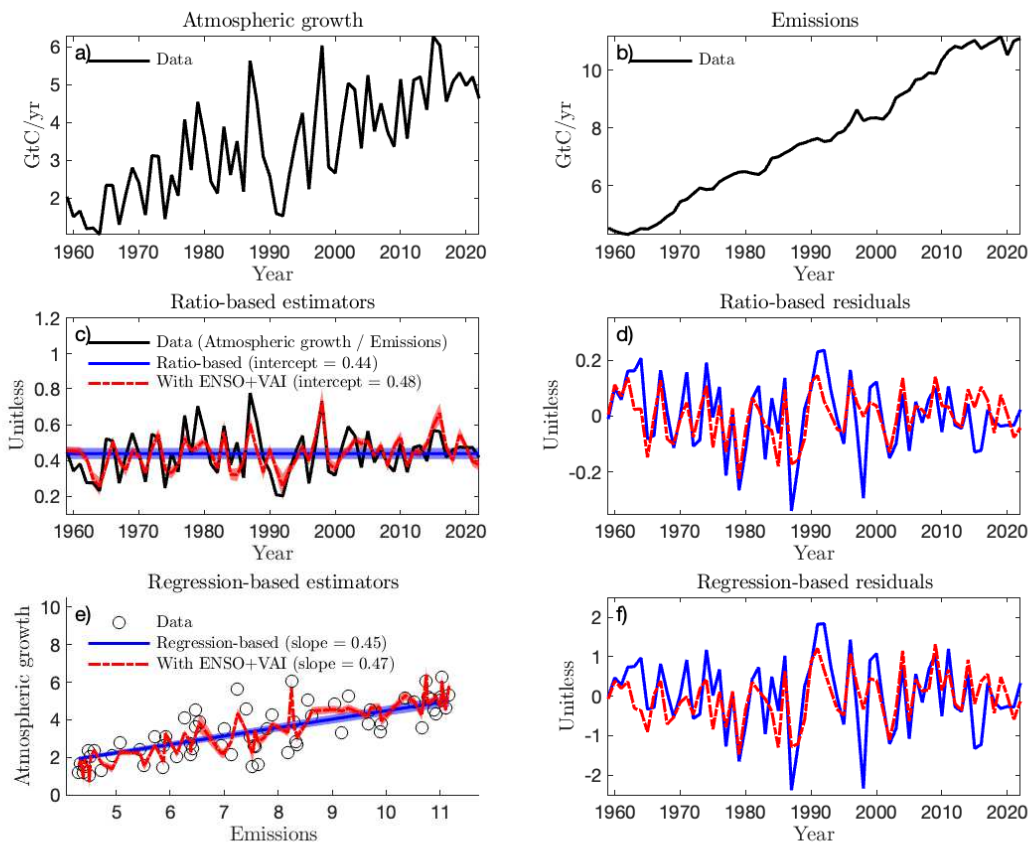
The cointegration analysis in S2.1 supports the hypothesis that the AF parameter α is constant during the period studied here (1959–2022). If the parameter α was changing in a specific direction, this would introduce a trend in the residuals u_t . The result from the Engle-Granger test shows that a trend is not present. This is confirmed graphically by the blue line in Figure 1f) and is in line with recent studies (Raupach et al., 2014; Bennedsen et al., 2019; Canadell et al., 2021; Bennedsen et al., 2023b). A Jarque-Bera test (Jarque and Bera, 1987) for normality of the estimated residuals for u_t results in a p -value of 24%, implying that we cannot reject the null of u_t having a Gaussian distribution.

A regression-based estimator of the airborne fraction

A ratio-based approach to estimating the AF takes its departure in the statistical model given by

$$\frac{G_t}{E_t} = \alpha + u_t^{(1)}, \tag{1}$$

Figure 1: a): Atmospheric concentration changes (G_t) and b): Emissions (E_t) data used in the study over the period 1959–2022. c): Data (G_t/E_t) in black, fit of (1) in blue (solid), fit of (3) in red (dashed), 95% confidence bands (shaded), “intercept” denotes the ratio-based estimate of the AF α . d): Ratio-based estimated residuals \hat{u}_t from (1) in blue (solid) and from (3) in red (dashed). e): Data (G_t) in circles, fit of (2) in blue (solid), fit of (4) in red (dashed), 95% confidence bands (shaded), “slope” denotes the regression-based estimate of the AF α . f) Regression-based estimated residuals \hat{u}_t from (2) in blue (solid) and from (4) in red (dashed).



where G_t are the yearly changes in atmospheric concentrations of CO_2 , E_t are yearly CO_2 emissions, the constant parameter α is the AF, and $u_t^{(1)}$ is the disturbance modelled as a zero-mean error process, for $t = 1, 2, \dots, T$, with T denoting the number of yearly observations in the sample. The disturbance $u_t^{(1)}$ captures deviations of the data G_t/E_t from the constant value α due to measurement errors and internal variability of the climate system. For the statistical model (1), it is straightforward to estimate the AF parameter α using the sample mean of the data G_t/E_t ,

yielding the *ratio-based estimator* as given by

$$\hat{\alpha}_1 = \frac{1}{T} \sum_{t=1}^T \frac{G_t}{E_t}.$$

The model in equation (1) expresses that, on average, the fraction α of emissions E_t is absorbed in the atmosphere, resulting in atmospheric concentrations increasing with the amount G_t . An alternative way to express this association between G_t and E_t is through the model formulation

$$G_t = \alpha E_t + u_t^{(2)}, \tag{2}$$

for $t = 1, 2, \dots, T$, where the disturbance $u_t^{(2)}$ is also a zero-mean error process. A model closely related to (2) has previously been used to reconstruct and predict CO₂ growth rates (Jones and Cox, 2005; Betts et al., 2016). The relationship between the disturbances in equations (1) and (2) is given by $u_t^{(1)} = u_t^{(2)} / E_t$. Cointegration of G_t and E_t implies that $u_t^{(2)}$ is a stationary process. Then, the parameter α can be estimated directly using a simple least-squares calculation, yielding the *regression-based estimator* as given by

$$\hat{\alpha}_2 = \left(\sum_{t=1}^T E_t^2 \right)^{-1} \sum_{t=1}^T E_t G_t.$$

Statistical properties of the two estimators

In the case of independent data, it is known that the regression-based estimator $\hat{\alpha}_2$ is efficient, i.e., it has lower estimation uncertainty compared to, for example, the ratio-based estimator $\hat{\alpha}_1$ (e.g., Cochran, 1977; Deng and Wu, 1987). We study this question for the case of cointegrated non-stationary time series in this paper, which is shown to be the relevant case for the AF in S2.1.

In the Supplementary Information (Section S1), we derive the asymptotic properties, that is, consistency and asymptotic normality, for the regression-based and the ratio-based estimators. These properties depend on the dynamics of CO₂ emissions, which are well-described by a random walk with drift over the sample 1959–2022, i.e. $E_t = E_0 + bt + x_t$, where $b > 0$ and x_t is a random walk (Supplementary Information S2.2).¹ In Proposition S1 of Section S1, we show that the regression-based estimator $\hat{\alpha}_2$ converges to the data-generating AF α at rate $T^{3/2}$, where T is

¹The variability of the differences in CO₂ emissions increases in the early 1990s (Supplementary Information, Figure S1). This is most likely due to increased variability of emission estimates from land-use and land-cover change, starting in the early 1990s (Supplementary Information S2.3). Below, we analyze the more recent subsample 1992–2022 as a robustness check, and we find that the results are similar to those obtained for the full sample.

the sample size. The ratio-based estimator $\hat{\alpha}_1$, on the other hand, converges to the data-generating AF α at the slower rate T , as is shown in Proposition S2. This implies that, when the sample size T is large, the estimation uncertainty in the regression-based estimator will be lower than in the ratio-based estimator, as in the case of independent data.

If the process E_t has positive probability density at zero, then the ratio-based estimator $\hat{\alpha}_1$ does not have a finite mean or variance, as Proposition S3 shows. This follows directly from the definition of $\hat{\alpha}_1$ as the sample mean of G_t/E_t : if values $E_t = 0$ have positive probability in the sample space, then the ratio G_t/E_t is not integrable on that space.

The maintained model assumption $E_t = E_0 + bt + x_t$ for CO₂ emissions implies positive probability density at zero, if x_t is a random walk of, for example, Gaussian increments. On the sample 1959–2022, however, the trend $E_0 + bt$ is much larger in magnitude than the random walk x_t , and it is not unreasonable to assume $x_t = 0$ for theoretical purposes. In this case, the ratio-based estimator $\hat{\alpha}_1$ has some standard statistical properties: It is an unbiased estimator of α , that is, the mean of $\hat{\alpha}_1$ equals α , and the variance of $\hat{\alpha}_1$ has a simple expression that can easily be estimated. However, we show in Proposition S4(i) that even in this case, a central limit theorem does *not* hold in general. The ratio-based estimator has a limiting Gaussian distribution only if we additionally assume that u_t is Gaussian, shown in Proposition S4(ii). In contrast, the regression-based estimator $\hat{\alpha}_2$ follows a central limit theorem with a limiting Gaussian distribution and the derivation does not require this additional assumption, as shown in Proposition S1.

Although the theoretical results show that the regression-based estimator $\hat{\alpha}_2$ is asymptotically, i.e., for sufficiently large T , more precise than the ratio-based estimator $\hat{\alpha}_1$, it is an empirical question which estimator is more precise in finite samples. In the next section, we estimate the variances of the regression-based and the ratio-based estimators on the historical sample and compare their magnitudes.

Estimating the airborne fraction over 1959–2022

We use time series data on yearly changes in atmospheric CO₂ (G_t), yearly CO₂ emissions from fossil fuels (E_t^{FF}), and yearly CO₂ emissions from land-use and land cover change (E_t^{LULCC}), for the sample 1959–2022. Total anthropogenic CO₂ emissions are then $E_t = E_t^{FF} + E_t^{LULCC}$. The data series are measured in gigatonnes of carbon per year (GtC/yr), obtained from the Global

Carbon Project² and presented in Figure 1a)–b).

The ratio-based estimate $\hat{\alpha}_1$ and the regression-based estimate $\hat{\alpha}_2$ are obtained from least-squares regressions applied to models (1) and (2), respectively. The fits are shown in Figure 1c) and 1e) and the associated estimated residuals \hat{u}_t are shown in 1d) and 1f), all as blue lines. To account for possible serial correlation and heteroskedasticity in the model errors u_t , we calculate standard errors using the heteroskedasticity and autocorrelation consistent (HAC) estimator of Newey and West (1987). The results are displayed in the first two columns of Table 1. The estimates largely agree on the magnitude of the AF, $\hat{\alpha}_1 = 43.86\%$ and $\hat{\alpha}_2 = 44.78\%$. However, the standard error of $\hat{\alpha}_2$ is 11% lower than the standard error of $\hat{\alpha}_1$, showing that the faster convergence rate of this estimator ($T^{3/2}$ versus T) outweighs the fact that the error process $u_t^{(2)}$ in (2) has a larger variance than the error process $u_t^{(1)}$ in (1). In particular, the estimated standard deviations (SDs) of these model errors are $\widehat{SD}(u_t^{(1)}) = 0.13$ and $\widehat{SD}(u_t^{(2)}) = 0.91$. The discrepancy is due to the different nature of the two models where $u_t^{(1)} = u_t^{(2)}/E_t$, with $E_t \gg 1$ in the sample 1959–2022.

Table 1: *Least-squares regression output of the linear models (1)–(4) for the Global Carbon Project data on the full sample 1959–2022 (left panel) and the subsample 1992–2022 (right panel). Estimates of the AF α are denoted by “ $\hat{\alpha}$ ”. The table reports standard errors “ $SE(\hat{\alpha})$ ” and standard errors relative to $SE(\hat{\alpha}_1)$ from model (1). Relative SE less than one indicates lower estimation uncertainty than the ratio-based estimator. The 95% confidence interval for the AF α , based on the Gaussian distribution, is denoted by “ $CI_{95\%}(\alpha)$ ”, the estimated standard deviation of the error u_t by “ $\widehat{SD}(u_t)$ ”, and the coefficient of determination by “ R^2 ”.*

	Full sample (1959-2022)				Recent sample (1992-2022)			
	(1)	(2)	(3)	(4)	(1)	(2)	(3)	(4)
$\hat{\alpha}$	0.4386	0.4478	0.4716	0.4697	0.4456	0.4497	0.4626	0.4613
$SE(\hat{\alpha})$	0.0159	0.0141	0.0126	0.0105	0.0190	0.0157	0.0124	0.0104
Relative SE	1.0000	0.8895	0.7904	0.6630	1.0000	0.8247	0.6509	0.5464
$CI_{95\%}(\alpha)$	[0.4074, 0.4697]	[0.4201, 0.4755]	[0.4470, 0.4962]	[0.4490, 0.4903]	[0.4083, 0.4828]	[0.4190, 0.4804]	[0.4384, 0.4869]	[0.4409, 0.4816]
$\widehat{SD}(u_t)$	0.1258	0.9088	0.0881	0.6292	0.1065	0.9309	0.0662	0.5891
R^2	0	0.5863	0.5258	0.8080	0	0.3558	0.6391	0.7592
ENSO included	No	No	Yes	Yes	No	No	Yes	Yes
VAI included	No	No	Yes	Yes	No	No	Yes	Yes

²Data from the Global Carbon Project can be found here: <https://www.icos-cp.eu/science-and-impact/global-carbon-budget/> last accessed June 17, 2024. The time series E_t^{FF} includes the cement carbonation sink, as described in Friedlingstein et al. (2023).

By introducing covariates in models (1) and (2), we can reduce the variance of the error processes u_t and thus achieve more precise estimates of the AF α . For example, it is common practice in the literature to control for the effects of El Niño ($ENSO_t$) and volcanic activity (VAI_t), (e.g. Raupach et al., 2008; van Marle et al., 2022).³ Hence, we consider the models

$$\frac{G_t}{E_t} = \alpha + \tilde{\gamma}_1 ENSO_t + \tilde{\gamma}_2 VAI_t + u_t^{(3)}, \quad (3)$$

$$G_t = \alpha E_t + \gamma_1 ENSO_t + \gamma_2 VAI_t + u_t^{(4)}, \quad (4)$$

for $t = 1, 2, \dots, T$, where $\tilde{\gamma}_i$ and γ_i , for $i = 1, 2$, are regression coefficients, and the model errors $u_t^{(j)}$ follow a zero-mean error process, for $j = 3, 4$. For both models, the coefficients can be estimated using least-squares regression. Let $\hat{\alpha}_3$ and $\hat{\alpha}_4$ denote the least-squares estimators of α from models (3) and (4), respectively. The estimation results relevant for the AF α are presented in columns labeled as (3) and (4) of Table 1, while the estimation results for the ENSO and VAI coefficients γ_i and $\tilde{\gamma}_i$, for $i = 1, 2$, are reported in Table S2 of the Supplementary Information. The regression fits of models (3) and (4) are presented as in Figure 1c) and 1e) and their associated estimated residuals \hat{u}_t in Figure 1d) and 1f), all as red dashed lines. The results show that controlling for the effects of ENSO and volcanic activity increases the estimate of the AF considerably, resulting in $\hat{\alpha}_3 = 47.16\%$ and $\hat{\alpha}_4 = 46.97\%$. The estimates of the standard deviations of the error terms ($\widehat{SD}(u_t^{(3)}) = 0.09$ and $\widehat{SD}(u_t^{(4)}) = 0.63$) decrease substantially compared to those of models (1) and (2), indicating that the covariates ENSO and VAI explain much variation in the data. This is corroborated by the coefficient of determination (R^2) values reported in Table 1.⁴ The decreased variance of the residuals from models (3) and (4) imply that their estimates of the constant AF α are more precise. The standard error of the estimate $\hat{\alpha}_4$ is approximately 16% lower than the one of estimate $\hat{\alpha}_3$ and approximately 34% lower than the one of the conventional estimate $\hat{\alpha}_1$. Our preferred estimate $\hat{\alpha}_4$ results in an estimated AF of 47.0% ($\pm 1.1\%$; 1σ) with an associated 95% confidence interval of [44.9%, 49.0%]. The slightly increased AF estimates for models (3) and (4), compared to the models (1) and (2) without covariates, confirm a similar finding in Betts et al.

³VAI data for volcanic activity are obtained from Ammann et al. (2003). ENSO data are constructed from the Niño 3 SST Index of the National Oceanic and Atmospheric Administration (NOAA), available at https://psl.noaa.gov/gcos_wgsp/Timeseries/Data/nino3.long.anom.data, last accessed June 17, 2024. We have converted monthly ENSO data into a yearly time series of September–August ENSO means (Jones et al., 2001). This 4-month lag provides the best fit between G_t and $ENSO_t$. The slight trend in yearly ENSO data is removed so that it has no impact on the AF estimates. The data are shown in Figure S2 of the Supplementary Information.

⁴The R^2 of model (1) equals zero by construction, since this model only features an intercept.

(2016).

As a robustness check, the right panel of Table 1 presents the results for the more recent subsample 1992–2022; Table S3 in the Supplementary Information contains the corresponding coefficient estimates for ENSO and VAI. Our conclusions for the full sample are corroborated by the results for the recent sample. All estimates of the AF α from the subsample are within the respective confidence bands of the estimates from the full sample, while the reductions in uncertainty from including the covariates and from using the regression-based estimator are similar.

Estimating the airborne fraction over 2023–2100

The approximate constancy of the AF over the historical period 1959–2022, as documented in the literature and confirmed by the cointegration analysis in this study, can be taken as the result of a near exponential growth in emissions and an approximately linear response of the carbon sinks to atmospheric concentrations (Raupach et al., 2014). In scenarios describing the future, for example when emissions are declining, the AF is expected to depart from constancy and may vary over time (e.g., Jones et al., 2013; Pressburger et al., 2023). This motivates the specification of a time-varying AF $\alpha = \alpha_t$, with α_t denoting the AF in year t , i.e. the fraction of emissions (E_t) added to the atmosphere (G_t) in year t .

The ratio-based model can then be written as

$$\frac{G_t}{E_t} = \alpha_t + u_t^{(1)},$$

where α_t is a yearly time-varying coefficient. The ratio G_t/E_t may be used to track the amount of emitted CO₂ that remains airborne, and hence, the estimate $\hat{\alpha}_{1,t} = G_t/E_t$ can be regarded as an appropriate but very noisy time-varying AF. A possible way to reduce the noise in AF is to apply a local smoothing operation, e.g. a two-sided moving average filter. In any case, filtered or not, the variability of the ratio G_t/E_t will be amplified when future emissions E_t start to approach zero. Another possible solution for noise reduction previously suggested in the literature, is to use the cumulative AF (CAF) in place of the yearly AF (e.g., Jones et al., 2013, 2016; Liddicoat et al., 2021). However, due to its cumulative nature, the CAF can be slow to detect changes in the behavior of the carbon sinks, making it less useful for the purpose of analyzing a time-varying AF (Supplementary Information S3).

When considering the regression-based model with a time-varying AF α_t , we obtain

$$G_t = \alpha_t E_t + u_t^{(2)}. \quad (5)$$

A versatile way of treating such a time-varying regression model is to assume random walk dynamics for α_t and estimate it by means of a recursive regression filter, such as the Kalman filter and smoother (Durbin and Koopman, 2012, §3.6.1, §4.3, §4.4). This approach yields the minimum mean-squared error estimator $\hat{\alpha}_{2,t}$, and it does not suffer from the deficiencies of the time-varying ratio-based estimator $\hat{\alpha}_{1,t}$. In the regression-based model (5), α_t is multiplied by E_t . When emissions turn negative for the first time in some year t , i.e. $E_t < 0$, we let α_t be reflected around one. For this purpose, we adjust the random walk specification at year t with a one-time instantaneous shift in α_t when $E_t < 0$ for the first time. Section S5 of the Supplementary Information provides further motivation and technical detail on this procedure.

To study the performance of the ratio-based $\hat{\alpha}_{1,t}$ and the regression-based $\hat{\alpha}_{2,t}$ estimators in situations where the AF is changing over time, we apply the two estimators to output from the MAGICC reduced-complexity climate model (Meinshausen et al., 2011). We let MAGICC produce future trajectories of G_t and E_t for $t = 2023, 2024, \dots, 2100$ according to the Shared Socioeconomic Pathways (SSPs; Riahi et al., 2017).⁵ We focus on the so-called SSP1-2.6 scenario, which is a high mitigation scenario consistent with a forcing level of 2.6 Wm^{-2} in the year 2100 (Riahi et al., 2017). Results obtained from other SSP scenarios are similar to those reported below and are presented in Section S5.1 of the Supplementary Information. Since MAGICC is a deterministic model without a stochastic representation of the climate variables, the trajectories of G_t and E_t generated by MAGICC are very smooth. To obtain output that resembles climate data, we perturb the trajectories of G_t and E_t by zero-mean Gaussian noise, where we set the variances equal to the estimates obtained on the historical data. These simulated trajectories, together with the original output from MAGICC and the historical Global Carbon Project data 1959–2022, are shown in panels a) and b) of Figure 2. Its panel c) presents the historical ratio G_t/E_t over 1959–2022 and the ratio-based and regression-based estimates $\hat{\alpha}_t$ of the time-varying airborne fraction over 2023–2100.

The ratio-based estimate $\hat{\alpha}_{1,t} = G_t/E_t$ (blue) is a very noisy series as we have anticipated, especially when $E_t \approx 0$. In contrast, the regression-based estimate $\hat{\alpha}_{2,t}$ (red) evolves over time

⁵The SSP scenarios can be run in MAGICC in a web browser via the link <https://live.magicc.org/scenarios/bced417f-0f7f-4bb7-8359-792a0a8b0368/overview>. Last accessed June 17, 2024.

in a stable fashion and shows sensible AF estimates, also when $E_t \approx 0$. A further benefit of the regression-based method is its delivery of confidence intervals for $\hat{\alpha}_{2,t}$ (shaded red area) which are not immediately available for the ratio-based estimator $\hat{\alpha}_{1,t}$. The covariates for El Niño and volcanic activity can readily be incorporated into the regression-based framework.

In the SSP1-2.6 scenario studied here, the regression-based AF estimate $\hat{\alpha}_{2,t}$ remains roughly constant until 2050, after which it gradually declines towards zero. In 2060, the atmospheric changes turn negative, resulting in a negative estimate of the AF, meaning that the sink uptake exceeds the emissions. In 2077, the emissions turn negative as well, instigating the visible switch to a positive estimate of the AF. The estimates of the AF exceed one from 2077 onwards, indicating that the sinks continue to absorb CO₂ even in this regime with highly negative emissions. These findings can be contrasted with the analysis of the SSP1-1.9 scenario (Supplementary Information, Figure S5) which has a similar trajectory for the regression-based AF estimates $\hat{\alpha}_{2,t}$ as for the SSP1-2.6 scenario, except that from 2080 onwards we have $\hat{\alpha}_{2,t} < 1$ implying that the sinks turn into carbon sources (releasing more carbon dioxide than they absorb).

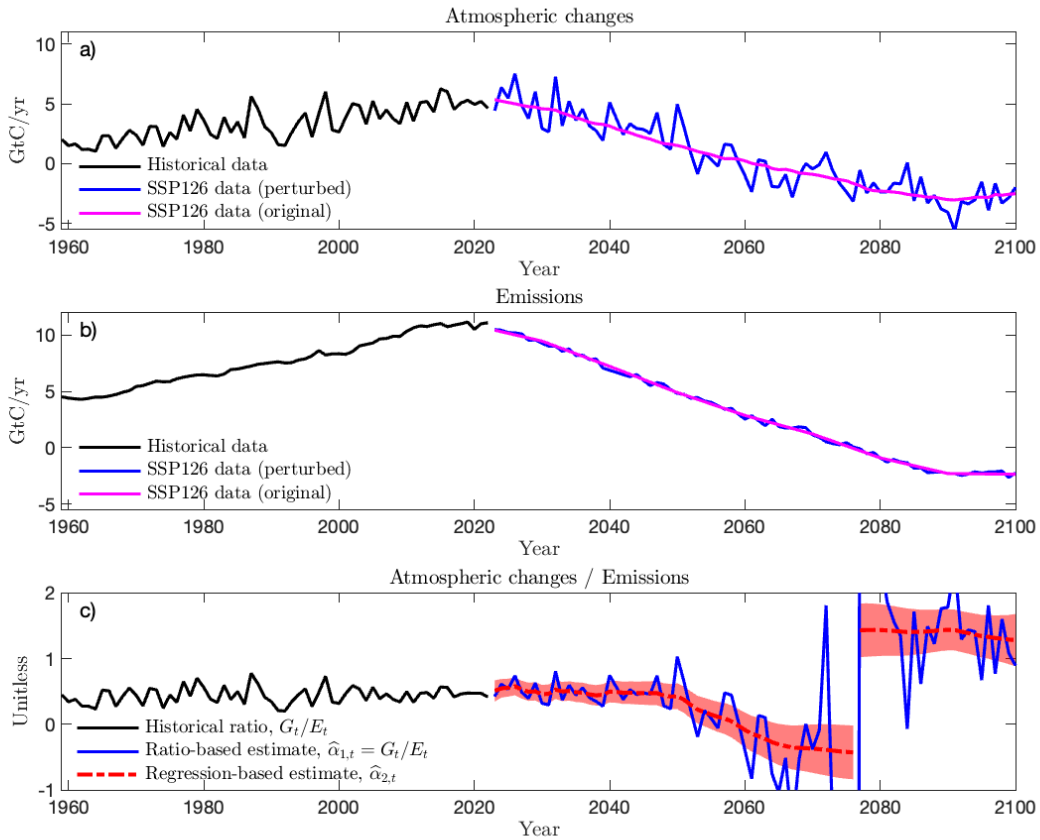
Discussion

Our empirical findings present a slightly higher AF than the consensus estimate of 44% (Canadell et al., 2021, p. 676) and the cumulative airborne fraction $CAF_t = 44.4\%$ (Supplementary Information S3) obtained from the Global Carbon Project data. The regression-based estimate of the AF, using the 1959-2022 sample of the Global Carbon Project data and controlling for El Niño and volcanic activity, is 47.0% ($\pm 1.1\%$; 1σ), with a 95% confidence interval of [44.9%, 49.0%].

When El Niño and volcanic activity are excluded from the analysis, the estimate is 44.8% ($\pm 1.4\%$; 1σ), which is more in line with the commonly reported results. When we apply the same analysis to two alternative data sets, we obtain slightly higher estimates of the AF than those from the Global Carbon Project (Supplementary Information S2.3). The more recent 1992–2022 subsample yields an AF estimate of approximately 46% ($\pm 1.0\%$; 1σ) for the Global Carbon Project data and slightly higher estimates for the two alternative data sets (Table 1 and Supplementary Information S2.4). To account for possible measurement error in G_t and E_t , we report Deming regressions (Deming, 1943) which are in line with the results reported so far (Supplementary Information S2.5). We may conclude that measurement error is not driving our results.

To summarize the theoretical findings in our study, we conclude that the ratio-based estimator

Figure 2: Analysis of SSP1-2.6 data over the period 2023–2100. a) Atmospheric concentration changes (G_t) for the historical period 1959–2022 (black) and the SSP period 2023–2100 (blue, magenta). b) Emissions (E_t) data. Magenta lines show the output from MAGICC; blue lines show the perturbed data. c) Ratio of atmospheric changes to emissions (G_t/E_t). The red line in c) is the estimated fraction of emissions (E_t) added to the atmosphere (G_t) in each year t , and, more specifically, it is the regression-based estimator $\hat{\alpha}_{2,t}$ of the time-varying airborne fraction α_t , obtained from the Kalman smoother. Shaded area is a 95% confidence band around $\hat{\alpha}_{2,t}$.



of the AF suffers from three main shortcomings. First, due to its definition as the ratio of changes in atmospheric concentrations to emissions, means and variances do not exist if zero emissions are possible. While this is of no concern on the historical sample, it is important when analyzing the AF on net-zero emissions scenarios. Studies of the past AF (such as Canadell et al., 2007; Raupach et al., 2008; Le Quéré et al., 2009; Knorr, 2009; Ballantyne et al., 2012; Raupach et al., 2014; Ballantyne et al., 2015; Keenan et al., 2016; Bennedsen et al., 2019; van Marle et al., 2022,

among others) are most likely not influenced to any substantial degree by this issue, but studies of future low-emission scenarios are affected (e.g. [Pressburger et al., 2023](#)). Second, we require stronger Gaussian assumptions on the distribution of the error process compared to the case of the regression-based estimator when a central limit theorem is invoked to compute confidence intervals and p -values based on a Gaussian distribution. Alternative methods such as the bootstrap can also be used for this purpose ([Efron and Tibshirani, 1993](#)). Again, studies on historical data are most likely not strongly affected by our findings, as Figure 1d suggests Gaussian residuals. Third, the ratio-based estimator converges to the data-generating AF at a slower rate than the regression-based estimator, even if zero-emissions are ruled out and errors are assumed to be normal. Both estimators converge faster than the common \sqrt{T} rate due to the non-stationarity of the two yearly time series variables emissions (E_t) and changes in atmospheric concentrations (G_t) and their cointegration. The ratio-based estimator converges at rate T and the regression-based estimator at rate $T^{3/2}$.

Our preferred regression-based estimator in this study has standard statistical properties, such as existence of first and second moments, it is defined for zero emissions, and it converges to the data-generating AF at a fast rate. A central limit theorem applies without assuming Gaussianity of the regression error, and confidence levels and p -values can be computed in the usual way. Based on theoretical arguments, on a simulation study ([Supplementary Information S4](#)), and on a historical sample of yearly data, we have shown that the regression-based estimator exhibits lower estimation uncertainty compared to the ratio-based estimator. Finally, we have argued that the regression-based estimator can readily be generalized to a time-varying AF specification with its estimations by means of the Kalman filter and smoother.

Table 2 summarizes the statistical tests performed in this study. The main empirical findings are: (1) emissions and changes in atmospheric concentrations cointegrate on the historical sample 1959–2022 with a constant regression coefficient, motivating the model choice for our theoretical studies, (2) the regression errors appear Gaussian, (3) the regression-based estimator has lower standard errors on the historical sample and in simulations than the ratio-based estimator, and (4) the findings are qualitatively the same on a subsample of the last 31 years. Further, we have provided evidence that measurement error in the two time series is not driving the results.

The main advantage of the regression-based estimator for a historical sample analysis is increased precision. In cases of net-zero emission scenarios and of future data analysis with emissions approaching zero, it will remain valid, unlike the ratio-based estimator. To illustrate this advan-

tage, we have simulated trajectories for emissions and changes in atmospheric concentrations over the period 2023–2100 consistent with SSP scenarios using the MAGICC reduced-complexity climate model. We regard this development as a first step and consider the use of climate projections from the Coupled Model Intercomparison Project (CMIP) as next steps in our research agenda.

Table 2: Summary of statistical tests

Test	Hypothesis of interest	Results
Dickey-Fuller (Dickey and Fuller, 1979)	Unit root in G_t, E_t	Confirmed
Engle-Granger (Engle and Granger, 1987)	Cointegration of G_t, E_t	Confirmed; AF constant on historical sample
Jarque-Bera (Jarque and Bera, 1987)	Normality of $u_t^{(2)}$ in $G_t = \alpha E_t + u_t^{(2)}$.	Confirmed
Sample split (1959–2022 vs. 1992–2022)	Robustness of results	Confirmed; AF constant on historical sample
Deming (Deming, 1943)	Robustness to measurement error in variables	Confirmed

Acknowledgements

We thank Morten Ø. Nielsen for helpful discussions regarding convergence of stochastic processes. M.B. gratefully acknowledges funding from the Independent Research Fund Denmark under grant no. 0219-00001B.

Author contributions

All authors contributed equally to the paper.

Data availability

Data are publicly available and can be found at

<https://github.com/mbennedsen/Regression-Approach-to-CO2-Airborne-Fraction>.

Code availability

MATLAB code for replication of all results in the main paper and Supplementary Information can be found at <https://github.com/mbennedsen/Regression-Approach-to-CO2-Airborne-Fraction>.

References

- Ammann, C. M., G. A. Meehl, W. M. Washington, and C. S. Zender (2003). A monthly and latitudinally varying volcanic forcing dataset in simulations of 20th century climate. *Geophysical Research Letters* 30(12).
- Bacastow, R. and C. D. Keeling (1973). Atmospheric carbon dioxide and radiocarbon in the natural cycle: Ii. changes from A. D. 1700 to 2070 as deduced from a geochemical model. In *Carbon and the biosphere conference proceedings; Upton, New York, USA*.
- Ballantyne, A. P., C. B. Alden, J. B. Miller, P. P. Tans, and J. W. C. White (2012). Increase in observed net carbon dioxide uptake by land and oceans during the past 50 years. *Nature* 488(7409), 70–72.
- Ballantyne, A. P., R. Andres, R. Houghton, B. D. Stocker, R. Wanninkhof, W. Anderegg, L. A. Cooper, M. DeGrandpre, P. P. Tans, J. B. Miller, C. Alden, and J. W. C. White (2015). Audit of the global carbon budget: estimate errors and their impact on uptake uncertainty. *Biogeosciences* 12(8), 2565–2584.
- Bennedsen, M., E. Hillebrand, and S. J. Koopman (2019). Trend analysis of the airborne fraction and sink rate of anthropogenically released CO₂. *Biogeosciences* 16(18), 3651–3663.
- Bennedsen, M., E. Hillebrand, and S. J. Koopman (2023a). A multivariate dynamic statistical model of the global carbon budget 1959–2020. *Journal of the Royal Statistical Society Series A: Statistics in Society* 186(1), 20–42.
- Bennedsen, M., E. Hillebrand, and S. J. Koopman (2023b). On the evidence of a trend in the CO₂ airborne fraction. *Nature* 616(7956), E1–E3.
- Betts, R. A., C. D. Jones, J. R. Knight, R. F. Keeling, and J. J. Kennedy (2016). El Niño and a record CO₂ rise. *Nature Climate Change* 6(9), 806–810.
- Canadell, J., P. Monteiro, M. Costa, L. C. da Cunha, P. Cox, A. Eliseev, S. Henson, M. Ishii, S. Jaccard, C. Koven, A. Lohila, P. Patra, S. Piao, J. Rogelj, S. Syampungani, S. Zaehle, and K. Zickfeld (2021). Global carbon and other biogeochemical cycles and feedbacks. In V. Masson-Delmotte, P. Zhai, A. Pirani, S. Connors, C. Péan, S. Berger, N. Caud, Y. Chen, L. Goldfarb, M. Gomis, M. Huang, K. Leitzell, E. Lonnoy, J. Matthews, T. Maycock, T. Waterfield, O. Yelekçi, R. Yu, and B. Zhou (Eds.), *Climate*

- Change 2021: The Physical Science Basis. Contribution of Working Group I to the Sixth Assessment Report of the Intergovernmental Panel on Climate Change*, pp. 673–816. Cambridge University Press, Cambridge, United Kingdom and New York, NY, USA.
- Canadell, J., D. Pataki, R. Gifford, R. Houghton, Y. Luo, M. Raupach, P. Smith, and W. Steffen (2007). Saturation of the terrestrial carbon sink. *Terrestrial Ecosystems in a Changing World*, 59–78.
- Canadell, J. G., C. Le Quéré, M. R. Raupach, C. B. Field, E. T. Buitenhuis, P. Ciais, T. J. Conway, N. P. Gillett, R. A. Houghton, and G. Marland (2007). Contributions to accelerating atmospheric CO₂ growth from economic activity, carbon intensity, and efficiency of natural sinks. *Proceedings of the National Academy of Sciences* 104(47), 18866–18870.
- Cochran, W. G. (1977). *Sampling Techniques* (3 ed.). New York: John Wiley.
- Davidson, J. and R. M. de Jong (1997). Strong laws of large numbers for dependent heterogeneous processes: a synthesis of recent and new results. *Econometric Reviews* 16(3), 251–279.
- de Jong, R. M. (1995). Laws of large numbers for dependent heterogeneous processes. *Econometric Theory* 11(2), 347–358.
- Deming, W. E. (1943). *Statistical adjustments of data*. Wiley New York.
- Deng, L.-Y. and C. F. J. Wu (1987). Estimation of Variance of the Regression Estimator. *Journal of the American Statistical Association* 82(398), 568–576.
- Dickey, D. A. and W. A. Fuller (1979). Distribution of the estimators for autoregressive time series with a unit root. *Journal of the American Statistical Association* 74(366a), 427–431.
- Durbin, J. and S. J. Koopman (2012). *Time Series Analysis by State Space Methods* (2 ed.). Oxford: Oxford University Press.
- Efron, B. and R. Tibshirani (1993). *An Introduction to the Bootstrap*. Chapman & Hall/CRC.
- Engle, R. F. and C. W. J. Granger (1987). Co-integration and error correction: Representation, estimation, and testing. *Econometrica* 55(2), 251–276.
- Fazekas, I. and O. Klesov (2001). A general approach to the strong law of large numbers. *Theory of Probability & Its Applications* 45(3), 436–449.
- Friedlingstein, P. (2015). Carbon cycle feedbacks and future climate change. *Philosophical Transactions of the Royal Society A* 373, 20140421.

Friedlingstein, P., M. O’Sullivan, M. W. Jones, R. M. Andrew, D. C. E. Bakker, J. Hauck, P. Landschützer, C. Le Quéré, I. T. Lujikx, G. P. Peters, W. Peters, J. Pongratz, C. Schwingshackl, S. Sitch, J. G. Canadell, P. Ciais, R. B. Jackson, S. R. Alin, P. Anthoni, L. Barbero, N. R. Bates, M. Becker, N. Bellouin, B. Decharme, L. Bopp, I. B. M. Brasika, P. Cadule, M. A. Chamberlain, N. Chandra, T.-T.-T. Chau, F. Chevallier, L. P. Chini, M. Cronin, X. Dou, K. Enyo, W. Evans, S. Falk, R. A. Feely, L. Feng, D. J. Ford, T. Gasser, J. Ghattas, T. Gkritzalis, G. Grassi, L. Gregor, N. Gruber, O. Gürses, I. Harris, M. Hefner, J. Heinke, R. A. Houghton, G. C. Hurtt, Y. Iida, T. Ilyina, A. R. Jacobson, A. Jain, T. Jarníková, A. Jersild, F. Jiang, Z. Jin, F. Joos, E. Kato, R. F. Keeling, D. Kennedy, K. Klein Goldewijk, J. Knauer, J. I. Korsbakken, A. Körtzinger, X. Lan, N. Lefèvre, H. Li, J. Liu, Z. Liu, L. Ma, G. Marland, N. Mayot, P. C. McGuire, G. A. McKinley, G. Meyer, E. J. Morgan, D. R. Munro, S.-I. Nakaoka, Y. Niwa, K. M. O’Brien, A. Olsen, A. M. Omar, T. Ono, M. Paulsen, D. Pierrot, K. Pocock, B. Poulter, C. M. Powis, G. Rehder, L. Resplandy, E. Robertson, C. Rödenbeck, T. M. Rosan, J. Schwinger, R. Séférian, T. L. Smallman, S. M. Smith, R. Sospedra-Alfonso, Q. Sun, A. J. Sutton, C. Sweeney, S. Takao, P. P. Tans, H. Tian, B. Tilbrook, H. Tsujino, F. Tubiello, G. R. van der Werf, E. van Ooijen, R. Wanninkhof, M. Watanabe, C. Wimart-Rousseau, D. Yang, X. Yang, W. Yuan, X. Yue, S. Zaehle, J. Zeng, and B. Zheng (2023). Global Carbon Budget 2023. *Earth System Science Data* 15(12), 5301–5369.

Gloor, M., J. L. Sarmienti, and N. Gruber (2010). What can be learned about carbon cycle climate feedbacks from the CO₂ airborne fraction? *Atmospheric Chemistry and Physics* 10, 7739 – 7751.

Granger, C. W. J. and P. Newbold (1974). Spurious regression in econometrics. *Journal of Econometrics* 2, 111 – 120.

Hamilton, J. D. (1994). *Time Series Analysis*. Princeton University Press.

Hill, M. R. (1999). Carbon dioxide emissions from the Russian Federation – problems and choices. *Energy & Environment* 10(1), 51–78.

Houghton, R. A. and A. Castanho (2023). Annual emissions of carbon from land use, land-use change, and forestry from 1850 to 2020. *Earth System Science Data* 15(5), 2025–2054.

Jarque, C. M. and A. K. Bera (1987). A test for normality of observations and regression residuals. *International Statistical Review* 2, 163–172.

Jones, C., E. Robertson, V. Arora, P. Friedlingstein, E. Shevliakova, L. Bopp, V. Brovkin, T. Hajima, E. Kato, M. Kawamiya, S. Liddicoat, K. Lindsay, C. H. Reick, C. Roelandt, J. Segsneider, and J. Tjiputra (2013). Twenty-First-Century Compatible CO₂ Emissions and Airborne Fraction Simulated by CMIP5 Earth System Models under Four Representative Concentration Pathways. *Journal of Climate* 26(13), 4398 – 4413.

- Jones, C. D., P. Ciais, S. J. Davis, P. Friedlingstein, T. Gasser, G. P. Peters, J. Rogelj, D. P. van Vuuren, J. G. Canadell, A. Cowie, R. B. Jackson, M. Jonas, E. Kriegler, E. Littleton, J. A. Lowe, J. Milne, G. Shrestha, P. Smith, A. Torvanger, and A. Wiltshire (2016). Simulating the Earth system response to negative emissions. *Environmental Research Letters* 11(9), 1–11.
- Jones, C. D., M. Collins, P. M. Cox, and S. A. Spall (2001). The Carbon Cycle Response to ENSO: A Coupled Climate–Carbon Cycle Model Study. *Journal of Climate* 14(21), 4113–4129.
- Jones, C. D. and P. M. Cox (2005). On the significance of atmospheric CO₂ growth rate anomalies in 2002–2003. *Geophysical Research Letters* 32(14).
- Karlin, S. and H. M. Taylor (1975). *A First Course in Stochastic Processes* (Second Edition ed.). Academic Press.
- Kaufmann, R. K. and D. I. Stern (2002). Cointegration analysis of hemispheric temperature relations. *Journal of Geophysical Research: Atmospheres* 107(D2).
- Keenan, T. F., I. C. Prentice, J. G. Canadell, C. A. Williams, H. Wang, M. Raupach, and G. J. Collatz (2016). Recent pause in the growth rate of atmospheric CO₂ due to enhanced terrestrial carbon uptake. *Nature communications* 7(1), 1–10.
- Klepper, S. and E. E. Leamer (1984). Consistent sets of estimates for regressions with errors in all variables. *Econometrica* 52(1), 163–183.
- Knorr, W. (2009). Is the airborne fraction of anthropogenic CO₂ emissions increasing? *Geophysical Research Letters* 36.
- Kuczmaszewska, A. (2005). The strong law of large numbers for dependent random variables. *Statistics & Probability Letters* 73(3), 305–314.
- Le Quéré, C., M. R. Raupach, J. G. Canadell, G. Marland, L. Bopp, P. Ciais, T. J. Conway, S. C. Doney, R. A. Feely, P. Foster, P. Friedlingstein, K. Gurney, R. A. Houghton, J. I. House, C. Huntingford, P. E. Levy, M. R. Lomas, J. Majkut, N. Metzl, J. P. Ometto, G. P. Peters, I. C. Prentice, J. T. Randerson, S. W. Running, J. L. Sarmiento, U. Schuster, S. Sitch, T. Takahashi, N. Viovy, G. R. van der Werf, and F. I. Woodward (2009). Trends in the sources and sinks of carbon dioxide. *Nature Geoscience* 2, 831 – 836.
- Le Quéré, C., C. Rödenbeck, E. T. Buitenhuis, T. J. Conway, R. Langenfelds, A. Gomez, C. Labuschagne, M. Ramonet, T. Nakazawa, N. Metzl, N. Gillett, and M. Heimann (2007). Saturation of the southern ocean CO₂ sink due to recent climate change. *Science* 316(5832), 1735–1738.

- Liddicoat, S. K., A. J. Wiltshire, C. D. Jones, V. K. Arora, V. Brovkin, P. Cadule, T. Hajima, D. M. Lawrence, J. Pongratz, J. Schwinger, R. Séférian, J. F. Tjiputra, and T. Ziehn (2021). Compatible Fossil Fuel CO₂ Emissions in the CMIP6 Earth System Models’ Historical and Shared Socioeconomic Pathway Experiments of the Twenty-First Century. *Journal of Climate* 34(8), 2853–2875.
- Meinshausen, M., S. C. B. Raper, and T. M. L. Wigley (2011). Emulating coupled atmosphere-ocean and carbon cycle models with a simpler model, MAGICC6 – Part 1: Model description and calibration. *Atmospheric Chemistry and Physics* 11(4), 1417–1456.
- Newey, W. K. and K. D. West (1987). A simple, positive semi-definite, heteroskedasticity and autocorrelation-consistent covariance matrix. *Econometrica* 55(394), 703–708.
- Park, J. Y. (1992). Canonical cointegrating regressions. *Econometrica* 60(1), 119–143.
- Phillips, P. C. B. and S. N. Durlauf (1986). Multiple time series regression with integrated processes. *The Review of Economic Studies* 53(4), 473–495.
- Phillips, P. C. B. and J. Y. Park (1988). Asymptotic equivalence of ordinary least squares and generalized least squares in regressions with integrated regressors. *Journal of the American Statistical Association* 83(401), 111–115.
- Piegorsch, W. W. and G. Casella (1985). The existence of the first negative moment. *The American Statistician* 39(1), 60–62.
- Pressburger, L., K. Dorheim, T. F. Keenan, H. McJeon, S. J. Smith, and B. Bond-Lamberty (2023). Quantifying airborne fraction trends and the destination of anthropogenic CO₂ by tracking carbon flows in a simple climate model. *Environmental Research Letters* 18(5).
- Raupach, M. R. (2013). The exponential eigenmodes of the carbon-climate system, and their implications for ratios of responses to forcings. *Earth System Dynamics* 4, 31 – 49.
- Raupach, M. R., J. G. Canadell, and C. L. Quéré (2008). Anthropogenic and biophysical contributions to increasing atmospheric CO₂ growth rate and airborne fraction. *Biogeosciences* 5, 1601 – 1613.
- Raupach, M. R., M. Gloor, J. L. Sarmiento, J. G. Canadell, T. L. Frölicher, T. Gasser, R. A. Houghton, C. Le Quéré, and C. M. Trudinger (2014). The declining uptake rate of atmospheric CO₂ by land and ocean sinks. *Biogeosciences* 11(13), 3453–3475.
- Riahi, K., R. Schaeffer, J. Arango, K. Calvin, C. Guivarch, T. Hasegawa, K. Jiang, E. Kriegler, R. Matthews, G. Peters, A. Rao, S. Robertson, A. Sebbit, J. Steinberger, M. Tavoni, and D. van Vuuren (2022). Mitigation pathways compatible with long-term goals. In P. Shukla, J. Skea, R. Slade, A. A. Khourdajie, R. van Diemen, D. McCollum, M. Pathak, S. Some, P. Vyas, R. Fradera, P. Shukla, J. Skea, R. Slade,

- A. A. Khourdajie, R. van Diemen, D. McCollum, M. Pathak, S. Some, P. Vyas, R. Fradera, M. Belkacemi, A. Hasija, G. Lisboa, S. Luz, and J. Malley (Eds.), *IPCC, 2022: Climate Change 2022: Mitigation of Climate Change. Contribution of Working Group III to the Sixth Assessment Report of the Intergovernmental Panel on Climate Change*. Cambridge University Press, Cambridge, UK and New York.
- Riahi, K., D. P. van Vuuren, E. Kriegler, J. Edmonds, B. C. O'Neill, S. Fujimori, N. Bauer, K. Calvin, R. Dellink, O. Fricko, W. Lutz, A. Popp, J. C. Cuaresma, S. KC, M. Leimbach, L. Jiang, T. Kram, S. Rao, J. Emmerling, K. Ebi, T. Hasegawa, P. Havlik, F. Humpenöder, L. A. Da Silva, S. Smith, E. Stehfest, V. Bosetti, J. Eom, D. Gernaat, T. Masui, J. Rogelj, J. Strefler, L. Drouet, V. Krey, G. Luderer, M. Harmsen, K. Takahashi, L. Baumstark, J. C. Doelman, M. Kainuma, Z. Klimont, G. Marangoni, H. Lotze-Campen, M. Obersteiner, A. Tabeau, and M. Tavoni (2017). The Shared Socioeconomic Pathways and their energy, land use, and greenhouse gas emissions implications: An overview. *Global Environmental Change* 42, 153–168.
- Rockström, J., O. Gaffney, J. Rogelj, M. Meinshausen, N. Nakicenovic, and H. J. Schellnhuber (2017). A roadmap for rapid decarbonization. *Science* 355(6331), 1269–1271.
- Roe, G. H. and M. B. Baker (2007). Why is climate sensitivity so unpredictable? *Science* 318(5850), 629–632.
- Schmith, T., S. Johansen, and P. Thejll (2012). Statistical analysis of global surface temperature and sea level using cointegration methods. *Journal of Climate* 25(22), 7822–7833.
- Siegenthaler, U. and H. Oeschger (1978). Predicting future atmospheric carbon dioxide levels. *Science* 199(4327), 388–395.
- van Marle, M. J. E., D. van Wees, R. A. Houghton, R. D. Field, J. Verbesselt, and G. R. van der Werf (2022). New land-use-change emissions suggest a declining CO₂ airborne fraction. *Nature* 603, 450–454.

Supplementary Information

A Regression-based Approach to the CO₂ Airborne Fraction: Enhancing Statistical Precision and Tackling Zero Emissions

S1 Theoretical analysis of the two estimators

Consider the cointegrated system

$$\begin{aligned} y_t &= \alpha z_t + u_t, \\ z_t &= z_0 + bt + x_t, \\ x_t &= \sum_{\tau=1}^t \xi_\tau, \end{aligned}$$

where $z_0, b \in \mathbb{R}$, u_t and ξ_t are covariance-stationary error terms, and $t = 1, 2, \dots, T$. In the context of the analysis of the AF, we have $y_t = G_t$ and $z_t = E_t$. Recall the two estimators of α :

$$\begin{aligned} \hat{\alpha}_1 &= \frac{1}{T} \sum_{t=1}^T \frac{y_t}{z_t}, \\ \hat{\alpha}_2 &= \left(\sum_{t=1}^T z_t^2 \right)^{-1} \sum_{t=1}^T z_t y_t. \end{aligned}$$

The second estimator $\hat{\alpha}_2$ has been thoroughly studied in the literature on cointegration. If $b = 0$, i.e. if there is no linear trend, then the stochastic trend x_t in z_t implies that $T(\hat{\alpha}_2 - \alpha)$ has a non-Gaussian limiting distribution (Phillips and Park, 1988). If $b \neq 0$, i.e., if there is a linear trend present in z_t , then the linear trend dominates the stochastic trend, which implies that $T^{3/2}(\hat{\alpha}_2 - \alpha)$ has a Gaussian limit. These results are well-known, see e.g. Park (1992), but for convenience we state the result relevant for the specific setting in this paper.

Proposition S1 (Park (1992)). *Let $b \neq 0$ and suppose that $\nu_t = (u_t, \xi_t)'$ is stationary and ergodic with zero-mean. Define $B_n(r) := n^{-1/2} \sum_{i=1}^{\lfloor nr \rfloor} \nu_i$ for $r \in [0, 1]$. Suppose that $B_n \xrightarrow{d} B$ such that B is a Brownian motion with $\text{Var}(B_1)$ positive definite. Then*

$$T^{3/2}(\hat{\alpha}_2 - \alpha) \xrightarrow{d} N(0, \sigma_2^2),$$

as $T \rightarrow \infty$, where $\sigma_2^2 > 0$.

Proof. The assumptions made on ν_t ensure that Assumption 2.1 in Park (1992) is satisfied. Since $b \neq 0$, Assumption 2.2 in Park (1992) also holds. The result now follows from Lemma 3.1 and Corollary 3.2 in Park (1992). □

Remark S1. When u_t is independent and identically distributed (*iid*), usual least-squares inference is valid, meaning that $\text{Var}(\hat{\alpha}_2)$ can be estimated by the usual least-squares estimator

$$\widehat{\text{Var}}(\hat{\alpha}_2) = \left(\sum_{t=1}^T z_t^2 \right)^{-1} T^{-1} \sum_{t=1}^T (y_t - \hat{\alpha}_2 z_t)^2.$$

If u_t may contain autocorrelation and heteroskedasticity, we can instead estimate $\text{Var}(\hat{\alpha}_2)$ using a heteroskedasticity and autocorrelation consistent (*HAC*) estimator, which is what we do in this study (Newey and West, 1987).

Remark S2. The conditions imposed on ν_t in Proposition S1 are rather weak and are satisfied for a large class of models. For instance, they are clearly satisfied if u_t and ξ_t are independent stationary and ergodic sequences. We refer to Phillips and Durlauf (1986) and references therein for various specific conditions ensuring the condition on ν_t holds.

The properties of the estimator $\hat{\alpha}_1$ are less well known. Indeed, to the best of our knowledge, the statistical properties of $\hat{\alpha}_1$ have not been studied previously. To this end, we write

$$\hat{\alpha}_1 = \frac{1}{T} \sum_{t=1}^T \frac{y_t}{z_t} = \alpha + \frac{1}{T} \sum_{t=1}^T \frac{u_t}{z_0 + bt + x_t} = \alpha + T^{-1} \sum_{t=1}^T U_t,$$

where $U_t = u_t/(z_0 + bt + x_t)$. We first show that $\hat{\alpha}_1$ is a superconsistent estimator of α .

Proposition S2. Let $b \neq 0$ and assume that u_t is *iid* with $\mathbb{E}(u_1) = 0$ and $\text{Var}(u_1) < \infty$, and that x_t obeys a strong law of large numbers, i.e. $t^{-1}x_t \xrightarrow{\text{a.s.}} 0$ as $t \rightarrow \infty$. Then, for all $\gamma > 0$, it holds that

$$T^{1-\gamma}(\hat{\alpha}_1 - \alpha) \xrightarrow{P} 0,$$

as $T \rightarrow \infty$.

Proof. Let $\epsilon, \delta > 0$ be given. Suppose, for ease of notation, that $b > 0$. The proof when $b < 0$ follows similar arguments. We want to show that

$$P(T^{1-\gamma}|\hat{\alpha}_1 - \alpha| \geq \epsilon) \leq \delta, \tag{S1.1}$$

for all T sufficiently large.

By assumption x_t obeys a strong law of large numbers. By the continuous mapping theorem, the same holds for $|x_t|$, meaning that $P(A) = 1$, where

$$A = \{\omega \in \Omega : \lim_{t \rightarrow \infty} t^{-1}|x_t(\omega)| = 0\}.$$

Let $T \geq 1$ and define the random variable

$$\tilde{x}_T := \sup_{t \geq T} t^{-1} |x_t|.$$

For all $\omega \in A$, we have $\lim_{t \rightarrow \infty} t^{-1} |x_t(\omega)| = 0$ and thus $\limsup_{t \rightarrow \infty} t^{-1} |x_t(\omega)| = \lim_{t \rightarrow \infty} t^{-1} |x_t(\omega)| = 0$. By the definition of limes superior, we get

$$\lim_{T \rightarrow \infty} \tilde{x}_T(\omega) := \lim_{T \rightarrow \infty} \sup_{t \geq T} t^{-1} |x_t(\omega)| = \limsup_{t \rightarrow \infty} t^{-1} |x_t(\omega)| = \lim_{t \rightarrow \infty} t^{-1} |x_t(\omega)| = 0.$$

Since $P(A) = 1$, we conclude that $\tilde{x}_T \xrightarrow{a.s.} 0$ as $T \rightarrow \infty$, which implies that

$$\sup_{t \geq T} t^{-1} |x_t| = \tilde{x}_T \xrightarrow{P} 0 \tag{S1.2}$$

as $T \rightarrow \infty$. Let $\nu \in (0, 1)$ and $T \geq 1$, and define the set

$$A_T = \left\{ \sup_{t \geq T} t^{-1} |x_t| \leq b\nu/2 \right\}.$$

The convergence in (S1.2) implies that there exists a $T_1 \geq 1$ such that $P(A_T) \geq 1 - \delta/2$ for all $T \geq T_1$. Likewise, since $z_0 \in \mathbb{R}$ is a constant, there exists a $T_2 \geq 1$ such that $\frac{|z_0|}{T} \leq b\nu/2$. Set $T_3 = \max(T_1, T_2)$, and write

$$\begin{aligned} T^{1-\gamma}(\hat{\alpha}_1 - \alpha) &= T^{-\gamma} \sum_{t=1}^T \frac{u_t}{z_0 + bt + x_t} \\ &= T^{-\gamma} \sum_{t=1}^{T_3} \frac{u_t}{z_0 + bt + x_t} + T^{-\gamma} \sum_{t=T_3+1}^T \frac{u_t}{z_0 + bt + x_t} \\ &= T^{-\gamma} B_{1, T_3} + T^{-\gamma} B_{T_3+1, T}, \end{aligned}$$

where $B_{s,r} := \sum_{t=s}^r \frac{u_t}{z_0 + bt + x_t}$. Since T_3 is fixed, there are only finitely many terms in B_{1, T_3} , and hence $T^{-\gamma} B_{1, T_3} \xrightarrow{P} 0$ as $T \rightarrow \infty$. For $B_{T_3+1, T}$, we write

$$\begin{aligned} T^{-\gamma} |B_{T_3+1, T}| &= T^{-\gamma} \left| \sum_{t=T_3+1}^T \frac{u_t}{z_0 + bt + x_t} \right| \\ &= T^{-\gamma} \left| \sum_{t=T_3+1}^T \frac{u_t}{bt} \frac{1}{1 + z_0 b^{-1} t^{-1} + x_t b^{-1} t^{-1}} \right| \\ &\leq T^{-\gamma} \sum_{t=T_3+1}^T \frac{|u_t|}{bt} \frac{1}{|1 + z_0 b^{-1} t^{-1} + x_t b^{-1} t^{-1}|}. \end{aligned}$$

Assuming that we are on A_{T_3} , we therefore have

$$T^{-\gamma}|B_{T_3+1,T}| \leq T^{-\gamma} \sum_{t=T_3+1}^T \frac{|u_t|}{bt} \frac{1}{|1-\nu|}.$$

This last term converges to zero in L^2 . To see this, note that

$$\begin{aligned} \text{Var} \left(T^{-\gamma/2} \sum_{t=T_3+1}^T \frac{|u_t|}{bt} \frac{1}{|1-\nu|} \right) &= T^{-\gamma} \sum_{t=T_3+1}^T \frac{\text{Var}(u_t)}{b^2 t^2} \frac{1}{(1-\nu)^2} \\ &\sim T^{-\gamma} \text{Var}(u_1) \sum_{t=T_3+1}^{\infty} \frac{1}{b^2 t^2} \frac{1}{(1-\nu)^2}, \end{aligned}$$

where the sum converges. This shows that $T^{-\gamma/2} \sum_{t=T_3+1}^T \frac{|u_t|}{bt} \frac{1}{|1-\nu|}$ converges in L^2 to a constant and thus that $T^{-\gamma}|B_{T_3+1,T}| \xrightarrow{L^2} 0$ as $T \rightarrow \infty$. We conclude that $T^{-\gamma} B_{T_3+1,T} \xrightarrow{P} 0$ as $T \rightarrow \infty$. Since this holds on A_{T_3} and $P(A_{T_3}) \geq 1 - \delta/2$, then, by choosing $T \geq T_3$ large enough, (S1.1) holds, which completes the proof. □

Remark S3. *It is straightforward to relax the assumption that u_t is iid, made in Proposition S2. In practice, we use a HAC estimator to estimate the variance of our estimators of $\hat{\alpha}_2$ to control for possible autocorrelation and heteroskedasticity in u_t .*

Remark S4. *The assumption in Proposition S2 that $x_t = \sum_{i=1}^t \xi_i$ obeys a strong law of large numbers is satisfied under quite mild conditions. For instance, it is satisfied if ξ_t is iid with finite variance (Kolmogorov's Law of Large Numbers), ξ_t is stationary and ergodic (the Ergodic Theorem, e.g. Karlin and Taylor, 1975, Theorem 9.5.5, p. 487), ξ_t is a mixingale (e.g. de Jong, 1995; Davidson and de Jong, 1997), or under certain mixing conditions on ξ_t (e.g. Fazekas and Klesov, 2001; Kuczmaszewska, 2005).*

Although $\hat{\alpha}_1$ is a superconsistent estimator of α , under what are arguably mild conditions, it is the case that U_t , and consequently $\hat{\alpha}_1$, does not possess any moments. This is, for example, the case if the denominator $z_0 + bt + x_t$ is a continuous random variable with positive probability density at zero. In such circumstances, $\mathbb{E}(\hat{\alpha}_1)$ and $\text{Var}(\hat{\alpha}_1)$ are not well-defined and talking about whether the estimator is, e.g., unbiased is meaningless. Although the results of non-existence of moments is well-known (e.g. Piegorsch and Casella, 1985), it may not be immediately obvious. We therefore state it as a proposition and provide a straightforward proof.

Proposition S3. *Let X be a random variable with continuous probability density function $f(x)$ such that $f(0) > 0$. Then $\mathbb{E}(X^{-\beta})$ does not exist for any $\beta \geq 1$.*

Proof. Note that because f is continuous and has $f(0) > 0$, then there exists an $\epsilon > 0$ such that $f(x) > 0$ for all $x \in [0, \epsilon]$. (If X cannot take positive values, then a similar arguments holds, but for $x \in [-\epsilon, 0]$.) Let $A := \inf_{x \in [0, \epsilon]} f(x) > 0$ and write

$$\mathbb{E}(|X|^{-\beta}) = \int_{-\infty}^{\infty} |x|^{-\beta} f(x) dx \geq \int_0^{\epsilon} |x|^{-\beta} f(x) dx \geq A \int_0^{\epsilon} x^{-\beta} dx = \infty$$

when $\beta \geq 1$. □

Remark S5. *Statistical issues with studying a ratio with a stochastic variable in the denominator have been encountered before in climate science. [Roe and Baker \(2007\)](#) discuss the “long tails” of the probability density function (PDF) for the climate sensitivity, i.e. the temperature response to a doubling of atmospheric CO_2 over its preindustrial value. They formulate the problem as $\Delta T = \lambda \cdot \Delta R_f$, where ΔT is the climate sensitivity and ΔR_f is the change in downward radiative flux, resulting from a doubling of CO_2 concentrations. The unknown parameter λ is given by $\lambda_0/(1 - f)$, where λ_0 is a “reference climate sensitivity” and f is the “total feedback factor”. It is clear that if f is a random variable such that the PDF of f is continuous with positive density at 1, then we are in a situation akin to the one studied in this paper and in Proposition S3. In fact, [Roe and Baker \(2007\)](#) rely on a number of published studies on the climate sensitivity and feedbacks in the climate system and argue that such a situation is likely. In their calculations, they assume that the distribution of f is Gaussian, which satisfies the conditions of a continuous PDF with positive density at 1. This leads to very long tails in the PDF of the climate sensitivity ΔT and, as our Proposition S3 shows, non-existence of moments.*

In the setting of this paper, we find that the deterministic term $z_0 + bt$ is quite large compared to the stochastic term x_t , implying that any probability density of the denominator $z_0 + bt + x_t$ at zero is likely very small. Hence, we proceed to study the estimator $\hat{\alpha}_1$ under the assumption that $x_t = 0$, i.e. that $z_t = z_0 + bt$ is a deterministic linear time trend. This avoids the problem of dividing by a random variable and thus of having a positive probability density at zero for the term in the denominator. Assume, for simplicity, that u_t is an iid sequence. In this case, we find that

$$\mathbb{E}(\hat{\alpha}_1) = \alpha,$$

and

$$\text{Var}(\hat{\alpha}_1) = T^{-2} \sum_{t=1}^T \mathbb{E}(U_t^2) = T^{-2} \sigma_u^2 \sum_{t=1}^T \frac{1}{(z_0 + bt)^2} \sim T^{-2} \sigma_u^2 c,$$

as $T \rightarrow \infty$, where $c = \sum_{t=1}^{\infty} \frac{1}{(z_0 + bt)^2}$ is a finite constant. Hence, in this case, we see that $\hat{\alpha}_1$ is an unbiased estimator of α , converging at the rate T^{-1} . However, the estimator does not obey a central limit theorem. To see this, write

$$T(\hat{\alpha}_1 - \alpha) = \sum_{t=1}^T \frac{u_t}{z_0 + bt}, \quad (\text{S1.3})$$

and observe that $\frac{u_t}{z_0 + bt} \xrightarrow{P} 0$ as $t \rightarrow \infty$, meaning that the first terms in the sum in (S1.3) dominate the entire sum, thus making central limit theorem-type results invalid. That is, we cannot conclude that $\hat{\alpha}_1$ is (asymptotically) Gaussian unless we impose an additional assumption that the error term u_t is itself Gaussian. For convenience, we again state these results formally.

Proposition S4. *Let $b \neq 0$ and assume that u_t is iid with $\mathbb{E}(u_1) = 0$ and $\text{Var}(u_1) < \infty$ and consider the sequence of random variables for $C_T = \sum_{t=1}^T \frac{u_t}{z_0 + bt}$, $T = 1, 2, \dots$. The following holds:*

- (i) *A central limit theorem does not hold in general for C_T , i.e. we cannot conclude that C_T has a Gaussian limit as $T \rightarrow \infty$.*
- (ii) *If $u_t \sim N(0, \sigma_u^2)$ with $\sigma_u^2 > 0$, then*

$$C_T \sim N(0, \sigma_{1,T}^2),$$

where $\sigma_{1,T}^2 = \sigma_u^2 \sum_{t=1}^T (z_0 + bt)^{-2}$, and, as $T \rightarrow \infty$,

$$C_T \xrightarrow{d} N(0, \sigma_1^2),$$

where $\sigma_1^2 = \sigma_u^2 \sum_{t=1}^{\infty} (z_0 + bt)^{-2}$.

Proof. (i) To see that a central limit theorem cannot hold in general, suppose that u_t is such that $\mathbb{E}(u_t^3) = s \neq 0$. Then

$$\mathbb{E}(C_T^3) = \sum_{t=1}^T \frac{\mathbb{E}(u_t^3)}{(z_0 + bt)^3} = s \sum_{t=1}^T \frac{1}{(z_0 + bt)^3} \rightarrow sc_3 \neq 0,$$

as $T \rightarrow \infty$, where $c_3 = \sum_{t=1}^{\infty} \frac{1}{(z_0 + bt)^3} < \infty$ and $c_3 \neq 0$. This shows that the asymptotic skewness of C_T is not zero, implying that the limiting distribution of C_T is not Gaussian.

(ii) That $C_T \sim N(0, \sigma_{1,T}^2)$ follows trivially by the assumption that u_t is iid Gaussian. The same holds for the second result. Formally, we may deduce it using characteristic functions. For $\theta \in \mathbb{R}$, we have

$$\mathbb{E}\left(e^{i\theta C_T}\right) = \prod_{t=1}^T \mathbb{E}\left(e^{i\frac{\theta}{z_0+bt}u_t}\right) = \prod_{t=1}^T e^{-\frac{1}{2}\frac{\theta^2\sigma_u^2}{(z_0+bt)^2}} = e^{-\frac{1}{2}\theta^2\sigma_u^2\sum_{t=1}^T\frac{1}{(z_0+bt)^2}} \rightarrow e^{-\frac{1}{2}\theta^2\sigma_1^2},$$

as $T \rightarrow \infty$, which concludes the proof. \square

In the case of the conventional estimator $\hat{\alpha}_1$, Proposition S4 shows that if we want to base inference on the normal distribution, we have to make distributional assumptions on the error term u_t . Indeed, if we are willing to assume that $u_t \sim N(0, \sigma_u^2)$, then we get

$$T(\hat{\alpha}_1 - \alpha) \sim N(0, \sigma_{1,T}^2),$$

and, as $T \rightarrow \infty$,

$$T(\hat{\alpha}_1 - \alpha) \xrightarrow{d} N(0, \sigma_1^2),$$

where $\sigma_{1,T}$ and σ_1^2 are as in Proposition S4(ii). Note that if u_t is iid, then $\sigma_{1,T}^2$ and σ_1^2 can be estimated directly from the sample variance of y_t/z_t . If u_t may contain autocorrelation and heteroskedasticity, we can instead estimate $\sigma_{1,T}^2$ and σ_1^2 using a HAC estimator, which is what we do in this study.

S2 Further empirical results

S2.1 Unit root and cointegration tests

Let y_t , $t = 1, 2, \dots, T$, be a time series and $L \geq 0$ an integer. We consider the following model for y_t for the null hypothesis,

$$y_t = a + y_{t-1} + \sum_{l=1}^L \beta_l \Delta y_{t-l} + \epsilon_t, \tag{S2.1}$$

where $a, \beta_1, \dots, \beta_L \in \mathbb{R}$ and ϵ_t is an error term. We use the convention that $\sum_{l=1}^L = 0$ if $L = 0$.

The model for y_t for the alternative hypothesis is

$$y_t = b + c \cdot t + \phi y_{t-1} + \sum_{l=1}^L \beta_l \Delta y_{t-l} + \epsilon_t, \tag{S2.2}$$

where $b, c \in \mathbb{R}$ and $\phi \in (-1, 1)$.

We use the Augmented Dickey-Fuller test (ADF; [Dickey and Fuller, 1979](#)) to test the null (H_0) that a data series is generated by the model in [\(S2.1\)](#) against the alternative (H_1) that the data series is generated by [\(S2.2\)](#). Depending on restrictions made on the three parameters a, b, c , this leads to three different tests:

1. AR: $a = b = c = 0$. This is the test for y_t having a unit root (H_0) against the alternative that y_t is an AR process.
2. ARD: $a = c = 0$. This is the test for y_t having a unit root (H_0) against the alternative that y_t is an AR process around a linear trend (i.e. that y_t is “trend-stationary”).
3. TS: This is the test for y_t having a unit root and a linear trend (H_0) against the alternative that y_t is a trend-stationary AR process.

We implement the ADF test using the built-in function `adftest` in the MATLAB Econometrics Toolbox. The p -values for testing H_0 against H_1 for these three tests and the two data series $y_t = G_t$ and $y_t = E_t$ are shown in the top six rows of [Table S1](#). For $y_t = E_t$ the p -values are very large regardless of the particular test conducted (AR, ARD, or TS) and the number of lags L used. Hence, there is strong evidence that E_t contains a stochastic trend. For $y_t = G_t$ the p -values are very large for the AR-test, regardless of the number of lags L used. For the ARD-test, the p -values are below 10% for $L = 0$ and $L = 1$ and very large for $L \geq 2$. For the TS-test, the p -values are below 10% regardless of the number of lags L used. Thus, the AR-test and ARD-test provide evidence that the time series of atmospheric CO₂ changes G_t contains a stochastic trend, while the TS-test indicates that the trend might be modelled using a deterministic trend $b + c \cdot t$. In summary, the ADF tests provide very strong evidence for the presence of trends in E_t and G_t and suggests that both series are non-stationary.

We next employ the Engle-Granger test ([Engle and Granger, 1987](#)) to test whether G_t and E_t are cointegrated. Formally, we consider the model

$$G_t = \alpha E_t + u_t \tag{S2.3}$$

and test whether the error term u_t is stationary. The parameter α is estimated by least-squares regression and the estimated residuals are computed,

$$\hat{u}_t = G_t - \hat{\alpha} E_t,$$

where $\hat{\alpha}$ is the least-squares estimate of α obtained from (S2.3). In a second step, we investigate whether the error terms u_t are stationary by performing the AR-version of the ADF test on the estimated residuals \hat{u}_t . The Engle-Granger test adjusts the critical values of the ADF test to account for the fact that the error term u_t is unobserved and that the estimated residuals \hat{u}_t are used in their place as data in the ADF test. We implement the Engle-Granger test using the built-in function `egcitest` in the MATLAB Econometrics Toolbox. The p -values for the Engle-Granger test are shown in the bottom row in Table S1. The null hypothesis of a unit root in u_t is firmly rejected for all lags L and we can therefore conclude that the two time series are cointegrated.

S2.2 Dynamics of CO₂ emissions over the 1959-2022 sample

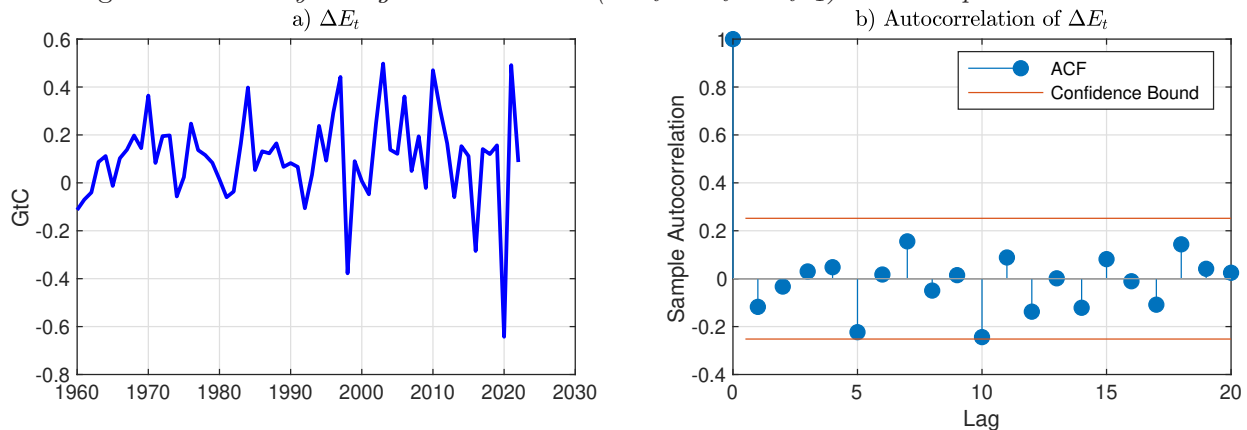
The theoretical properties of the estimators of the AF depend on the dynamics of the emissions E_t , as discussed in Section S1. Section S2.1 found that emissions are non-stationary. This section further explores the dynamics of the emissions over the sample period 1959–2022.

Figure S1 motivates a random walk with drift as an appropriate model for emissions. Panel a) shows the differences of yearly CO₂ emissions, $\Delta E_t = E_t - E_{t-1}$, for $t = 2, \dots, T$. They are well described by a constant plus a stationary, zero-mean error term, say, $\Delta E_t = b + \xi_t$. Panel b) shows that the autocorrelation function of the differences in emissions is not statistically significant at all lags (except 0), and thus the error term ξ_t is white noise. Therefore, our model for CO₂ emissions E_t is a random walk with drift b . We write $E_t = E_{t-1} + b + \xi_t$, or, equivalently, $E_t = E_0 + b \cdot t + x_t$, where $x_t = \sum_{\tau=1}^t \xi_\tau$ is the random walk process $x_t = x_{t-1} + \xi_t$ without drift, and E_0 are initial emissions.

The constant b can be estimated directly as the sample mean of ΔE_t , and on the sample 1959–2022, we find $\hat{b} = 0.1043$ (standard error 0.0241). This estimate is close to the corresponding estimate found in Bennedsen et al. (2023a) using a dynamic statistical system model for the Global Carbon Budget. A Jarque-Bera test (Jarque and Bera, 1987) for normality of the estimated residuals $\hat{\xi}_t = \Delta E_t - \hat{b}$ results in a p -value below 0.1%, meaning that we can reject that ξ_t is a Gaussian process.

Figure S1a) shows that the variability of the differences in CO₂ emissions increases in the early 1990s. This is most likely due to increased variability of emission estimates from land-use and land-cover change, starting in the early 1990s (see Supplementary Information S2.3 and also van Marle et al., 2022). In the main paper, we analyze the more recent subsample 1992–2022 as a robustness check, and we find results very similar to those obtained for the full 1959-2022 sample.

Figure S1: Yearly changes in emissions ($\Delta E_t = E_t - E_{t-1}$) over the period 1960–2022.



S2.3 Analysis of alternative data sets

We use data on yearly changes in atmospheric CO_2 (G_t), yearly CO_2 emissions from fossil fuels (E_t^{FF}), and yearly CO_2 emissions from land-use and land cover change (E_t^{LULCC}). Total anthropogenic CO_2 emissions are then $E_t = E_t^{FF} + E_t^{LULCC}$. The uncertainty in measurements of the AF stems in large part from uncertainties in the magnitude of LULCC emissions (van Marle et al., 2022). We therefore follow van Marle et al. (2022) and estimate the AF using three different data sets for LULCC emissions (GCP, H&C, vMa), while data for atmospheric CO_2 changes and CO_2 emissions from fossil fuels are obtained from the most recent edition of the Global Carbon Budget data set (Friedlingstein et al., 2023).⁶ The GCP LULCC data are from the Global Carbon Project (Friedlingstein et al. (2023)), the H&C LULCC data are from Houghton and Castanho (2023), and the vMa LULCC data are from van Marle et al. (2022). We thus have three different data sets, only differing in the LULCC time series. The data are available for the period 1959–2022 (Figure S2).

Estimation results for α using the alternative data sets are reported in Table S2. For ease of comparison, we also include the results presented in Table 1 using the GCP data set. The table shows that the overall estimates of α vary across the three data sets, with the GCP data generally resulting in lower estimates of the AF than the H&C and vMa data, a result of the H&C and vMa LULCC data being significantly below the GCP LULCC data over 1959–2022 (Figure S2). The reduction in uncertainty obtained by using $\hat{\alpha}_2$ instead of $\hat{\alpha}_1$ is of the same magnitude across the

⁶Data from the Global Carbon Project can be found at <https://www.icos-cp.eu/science-and-impact/global-carbon-budget/2023> last accessed June 17, 2024. Data for the various LULCC time series can be found at <https://doi.org/10.7910/DVN/U7GHRH> and <https://github.com/mbennedsen/Regression-Approach-to-CO2-Airborne-Fraction>, last accessed June 17, 2024.

three data sets, however.

S2.4 Analysis of the subsample 1992–2022

In this section, we analyze the AF over the recent subsample 1992-2022 for all three data sets. The subsample analysis is motivated by the contradictory findings of trends in the AF mentioned in the introduction, the possibility of a structural break in the data around 1990 (Bennedsen et al., 2023b), substantial disagreements in land-use and land-cover change emissions data before 1992 (van Marle et al., 2022, see also Figure S2), and the presumption of better data quality in the latter part of the sample (e.g. Hill, 1999).

The estimation results are shown in Table S3. The results show estimates of α that are within the confidence intervals from the full-sample analysis (Table S2), although the estimates coming from the most recent sample 1992–2022 are slightly below those from the entire sample 1959–2022.

We find that the regression-based estimator $\hat{\alpha}_2$ improves the precision, measured by the standard error of the estimator, by approximately 18% compared to the conventionally used ratio-based estimator $\hat{\alpha}_1$. Including data on ENSO and volcanic activity in the analysis, the regression-based estimator $\hat{\alpha}_4$ improves the precision with approximately 45%, compared to the ratio-based estimator of the AF $\hat{\alpha}_1$. Using data from the Global Carbon Project (e.g. Friedlingstein et al., 2023), our best estimate of the AF is 46.1% with an associated standard error of 1.0%, resulting in a 95% confidence interval of [44.1%, 48.2%] for the AF. As was the case for the full sample studied in Section S2.3, the alternative LULCC data results in higher estimates of the AF than the LULCC coming from the GCP data.

S2.5 Accounting for potential measurement errors in the data

It is likely that measurement errors are present in both the left-hand side variable G_t and the right-hand side variable E_t of the regression (2). It is well-known that measurement errors may lead to biases in parameters estimates (e.g. Klepper and Leamer, 1984). As a robustness check, we run a so-called *Deming regression* (Deming, 1943) which is a regression that takes potential measurement errors into account when formulating the regression-based estimator.

Formally, we assume that the data G_t and E_t are noisy measurements of the variables G_t^* and E_t^* , where

$$G_t^* = \alpha E_t^* + u_t \tag{S2.1}$$

and

$$\begin{aligned} G_t &= G_t^* + \epsilon_{G,t}, & \epsilon_{G,t} &\overset{iid}{\sim} N(0, \sigma_{G,1}^2), \\ E_t &= E_t^* + \epsilon_{E,t}, & \epsilon_{E,t} &\overset{iid}{\sim} N(0, \sigma_{E,1}^2), \end{aligned}$$

with $\epsilon_{G,t}$ and $\epsilon_{E,t}$ being statistically independent. Let $\delta = \sigma_{G,1}^2/\sigma_{E,1}^2$ denote the ratio of the two measurement error variances. Then the Deming regression estimate of α in (S2.1) using the data G_t and E_t is

$$\hat{\alpha}_{deming} = \frac{M_{GG} - \delta M_{EE} + \sqrt{(M_{GG} - \delta M_{EE})^2 + 4\delta M_{EG}^2}}{2M_{EG}}, \quad (\text{S2.2})$$

where

$$\begin{aligned} M_{GG} &= \frac{1}{T} \sum_{t=1}^T G_t^2, \\ M_{EE} &= \frac{1}{T} \sum_{t=1}^T E_t^2, \\ M_{EG} &= \frac{1}{T} \sum_{t=1}^T E_t G_t. \end{aligned}$$

We apply the Deming estimator (S2.2) to the three data sets (GCP, H&C, vMa) and two subsamples (1959–2022 and 1992–2022). Since the measurement error ratio δ is unknown, we run the regression for several values of δ , namely $\delta \in \{0.2, 0.5, 1, 2, 5\}$. The results are shown in Table S4. Comparing with the estimates $\hat{\alpha}_2$ obtained from Equation (2) and reported in Tables S2 and S3, we see that although the Deming estimates are slightly larger than those obtained from the regression-based estimator $\hat{\alpha}_2$, the Deming estimates are always within the confidence bands of the regression-based estimator $\hat{\alpha}_2$, suggesting that potential measurement error is not driving the results reported in this study.

S3 Cumulative airborne fraction

Another alternative to the ratio-based and regression-based estimators of the AF is the *cumulative airborne fraction* (CAF) estimator, defined as the ratio of the cumulative changes in atmospheric CO₂ concentrations and the cumulative CO₂ emissions, given by

$$\text{CAF}_{t_0,t} = \frac{\sum_{j=t_0}^t G_j}{\sum_{j=t_0}^t E_j}, \quad (\text{S3.1})$$

where t_0 denotes the first year of the sample and t is the current year or the last year of the sample. Using the Global Carbon Project data 1959–2022, we can calculate the CAF, yielding

$$\text{CAF}_{1959,2022}^{\text{GCP}} = \frac{\sum_{j=1959}^{2022} G_j}{\sum_{j=1959}^{2022} E_j} = \frac{218.03}{491.03} = 44.40\%.$$

The two alternative data sets, introduced in Section S2.3, result in

$$\text{CAF}_{1959,2022}^{\text{H\&C}} = \frac{\sum_{j=1959}^{2022} G_j}{\sum_{j=1959}^{2022} E_j} = \frac{218.03}{457.65} = 47.64\%,$$

and

$$\text{CAF}_{1959,2022}^{\text{vMa}} = \frac{\sum_{j=1959}^{2022} G_j}{\sum_{j=1959}^{2022} E_j} = \frac{218.03}{442.07} = 49.32\%.$$

Due to its cumulative nature, the CAF is not as useful for studying changes and trends in the AF, when compared to the ratio- and regression-based measures considered in the main paper, which utilize the yearly variables G_t and E_t . To illustrate this point, Figure S3 shows the CAF over the period 2023–2100 using the data from the SSP1-2.6 scenario, i.e. the same data as used in Figure 2 of the main paper. Panel a) of the figure shows the $\text{CAF}_{2023,t}$ $t = 2023, 2024, \dots, 2100$, as defined in Equation (S3.1). As can be seen, the CAF is very smooth and generally adjusts slowly to changes in the behavior of the carbon system.

A possible remedy to the “over-smoothness” is to calculate the CAF over a (smaller) fixed window of length $w \geq 1$. Consider therefore the alternative CAF, defined as

$$\text{CAF}_{t_0,t}(w) = \text{CAF}_{\max\{t_0-w+1,t_0\},t} = \frac{\sum_{j=\max\{t_0-w+1,t_0\}}^t G_j}{\sum_{j=\max\{t_0-w+1,t_0\}}^t E_j}, \quad (\text{S3.2})$$

for a window length $w \geq 1$. This is the “moving-window” version of the CAF, where each data point is calculated using only the preceding w years (when $t - t_0 + 1 < w$, then $t - t_0 + 1$ years are used). For instance, $w = 1$ corresponds to the conventional ratio-based AF as considered in the main paper, while $w = 78$ is the CAF suggested in Equation (S3.1) above (because there are 78 yearly data points in the 2023–2100 SSP data). For other values of w , but with $1 < w < 78$, the CAF(w) in (S3.2) is calculated using the cumulative data using shorter windows. This resulting CAF may be able to track the changes and trends in the AF better.

If w is chosen too large, the CAF in (S3.2) will inherit the downsides of the “full-sample” CAF in (S3.1), i.e. it will be slow to adapt. Conversely, in case w is too small, this version of the CAF inherits the downsides of the ratio-based estimator considered in the main paper since it is

still defined as a ratio. To illustrate these points, Panels b)–f) of Figure S3 show $\text{CAF}_{2023,t}(w)$, $t = 2023, 2024, \dots, 2100$, for $w = 50, 20, 10, 5, 1$, respectively. In particular, when choosing a smaller window size w , the CAF is indeed tracking the changes in the behavior of the carbon system more closely, while it also has the effect of making the CAF vulnerable to periods where $\sum E_t \approx 0$.

S4 Simulation study: Performance of the estimators in conditions similar to the data sample 1959–2022

We simulate data from the models in (1)–(2). To facilitate comparison, we set the data-generating value of α to 0.4386, which is the estimated value obtained using the model in (1) and the GCP data set, see Table 1. The variance of the error terms are set to $\text{Var}(\epsilon_t^{(1)}) = 0.1258^2$ and $\text{Var}(u_t^{(2)}) = 0.9088^2$, again corresponding to the estimates from the GCP data (Table 1). Using these values, we simulate data $y_t = G_t/E_t$ from model (1) directly. To simulate from model (2), we first need to simulate an emissions trajectory. To this end, we specify emissions as a random walk plus drift, i.e. $E_t = E_{t-1} + b + \xi_t$, where b is drift parameter, as motivated in this study.

Using the GCP data for 1959–2022, we estimate b and $\text{Var}(\xi_t)$ from the model $\Delta E_t := E_t - E_{t-1} = b + \xi_t$. We also set $E_0 = 4.3433$, which is the first observation of E_t from the GCP data. Then, we simulate emissions time series using the dynamic equation $E_t = E_{t-1} + \hat{b} + \xi_t$, $t = 1, 2, \dots, T$, where the variance of ξ_t is set to the value $\widehat{\text{Var}}(\xi_t)$ found on the GCP data.

We simulate 10^6 instances of G_t and E_t for $t = 1, 2, \dots, T$. For each instance, we estimate α using the estimators $\hat{\alpha}_1$ and $\hat{\alpha}_2$, and calculate the squared errors of the resulting estimates. The root mean squared errors (RMSE) of the two estimators are obtained by averaging the squared errors over the 10^6 simulations. We run these simulation studies for various sample sizes, namely $T = 64, 65, \dots, 142$. $T = 64$ corresponds to the sample size relevant for the data in the main paper (1959–2022), while $T = 142$ corresponds to data until 2100 (1959–2100). The RMSEs of the two estimators, as functions of sample size T , are shown in the left plot of Figure S4. The relative RMSE, i.e. $\text{RMSE}(\hat{\alpha}_2)/\text{RMSE}(\hat{\alpha}_1)$, as a function of T , is shown in the right plot of Figure S4.

From the left plot of Figure S4, we see that the RMSE of both estimators are decreasing in T . The decrease is much more pronounced for the estimator $\hat{\alpha}_2$ compared to the estimator $\hat{\alpha}_1$. This is to be expected, since we saw above that $\hat{\alpha}_2$ converges to α at the rate $T^{3/2}$, while $\hat{\alpha}_1$ converges at the slower rate $T^{1-\gamma}$, $\gamma > 0$. The difference between the performance of the two estimators is illustrated in the right plot of Figure S4, where the relative RMSE is shown. For $T = 64$,

corresponding to the leftmost observation, the RMSE of $\hat{\alpha}_2$ is approximately 10% lower than the RMSE of $\hat{\alpha}_1$. These simulation results align with the empirical estimates, where it was found that $\hat{\alpha}_2$ was approximately 10% more precise than $\hat{\alpha}_1$ (Tables 1 and S2). The relative performance continues to diverge as the sample size gets larger; for $T = 142$, the reduction in RMSE is on the order of 50%.

S5 Details on the Kalman filter approach to estimating the time-varying airborne fraction

Consider the state-space model

$$G_t = \alpha_t E_t + u_t^{(2)}, \quad u_t^{(2)} \stackrel{iid}{\sim} N(0, \sigma_u^2),$$

$$\alpha_{t+1} = \begin{cases} \alpha_t + \eta_t & \text{if } t + 1 \neq \tau, \\ 1 - \alpha_t + \eta_t & \text{if } t + 1 = \tau, \end{cases}, \quad \eta_t \stackrel{iid}{\sim} N(0, \sigma_\eta^2),$$

where E_t is treated as a covariate (exogenous variable) and τ denotes the year where emissions first turn negative, i.e. $\tau = \inf\{t : E_t < 0\}$. (We use the convention that if $\{t : E_t < 0\}$ is empty, then $\tau = \infty$.) This is a random walk model for α_t , i.e. $\alpha_{t+1} = \alpha_t + \eta_t$, for all years t except at the year $t + 1 = \tau$, where the transition equation becomes $\alpha_{t+1} = 1 - \alpha_t + \eta_t$.⁷

Given the data for G_t , we may use the Kalman filter to evaluate the likelihood of the model. The parameters σ_u^2 and σ_η^2 may be estimated by the method of maximum likelihood, and the Kalman smoother provides an estimate of the time-varying parameter α_t , namely $\hat{\alpha}_{2,t} = \hat{\mathbb{E}}(\alpha_t | \text{data})$, where “data” denotes (G_t, E_t) for $t = 2023, 2024, \dots, 2100$. Similarly, the Kalman smoother provides confidence bands around $\hat{\alpha}_{2,t}$. We refer to Durbin and Koopman (2012) for a textbook treatment of state space models and the Kalman filter and smoother.

S5.1 Application to SSP scenarios 2023-2100

Figures S5–S9 present the results from applying the regression based estimator $\hat{\alpha}_{2,t} = \hat{\mathbb{E}}(\alpha_t | \text{data})$ of the time-varying airborne fraction α_t , obtained from the Kalman smoother, to scenarios SSP1-1.9,

⁷The reason for specifying the model in a way that reflects α_t around one at $t = \tau$ is as follows: When $G_t < 0$ and $E_t > 0$ we expect that $\alpha_t < 0$, which means that the carbon sinks absorb more than is emitted. When emissions turn negative, i.e. $E_t < 0$, then α_t switches to being positive. Because we still expect that the sinks absorb more than what is emitted, we would in fact expect that $\alpha_t > 1$. This feature is obtained by the specification $\alpha_\tau = 1 - \alpha_{\tau-1} + \eta_\tau$.

SSP2-4.5, SSP3-7.0, SSP4-3.4, and SSP5-8.5, respectively. The SSP scenarios were run using the simple climate model MAGICC (Meinshausen et al., 2011).⁸

⁸The SSP scenarios can be run in MAGICC in a web browser via the link <https://live.magicc.org/scenarios/bced417f-0f7f-4bb7-8359-792a0a8b0368/overview>. Last accessed June 17, 2024.

Table S1: *p*-values for the Augmented Dickey-Fuller (ADF) test for a unit root and the Engle-Granger test for cointegration between G_t and E_t on the GCP data (1959–2022), see Section S2.1 for details. First six rows are ADF tests and the last row is the Engle-Granger test. “AR”: The null model is a unit root model while the alternative model is an AR model. “ARD”: The null model is a unit root model while the alternative model is an AR model with drift. “TS”: The null model is a unit root model with a constant (i.e. a drift in levels) while the alternative model is an AR model with a time trend. “Engle-Granger”: The null hypothesis is that the error term u_t in $G_t = \alpha E_t + u_t$ has a unit root, i.e. that G_t and E_t are not cointegrated. The value “ L ” denotes the number of lags included in both the null and alternative models, see equations (S2.1)–(S2.2).

	$L = 0$	$L = 1$	$L = 2$	$L = 3$	$L = 4$	$L = 5$
$y_t = G_t$ (AR)	0.2349	0.4867	0.6597	0.7982	0.8403	0.8470
$y_t = G_t$ (ARD)	0.0039	0.0778	0.3105	0.4384	0.4564	0.3895
$y_t = G_t$ (TS)	0.0010	0.0010	0.0035	0.0192	0.0231	0.0056
$y_t = E_t$ (AR)	0.9990	0.9990	0.9990	0.9990	0.9953	0.9984
$y_t = E_t$ (ARD)	0.9488	0.9329	0.9038	0.8533	0.8201	0.8871
$y_t = E_t$ (TS)	0.0933	0.2108	0.3108	0.3339	0.2250	0.4775
Engle-Granger	0.0010	0.0010	0.0019	0.0135	0.0173	0.0038

Figure S2: Data used in the study over the period 1959–2022. The dashed vertical black line

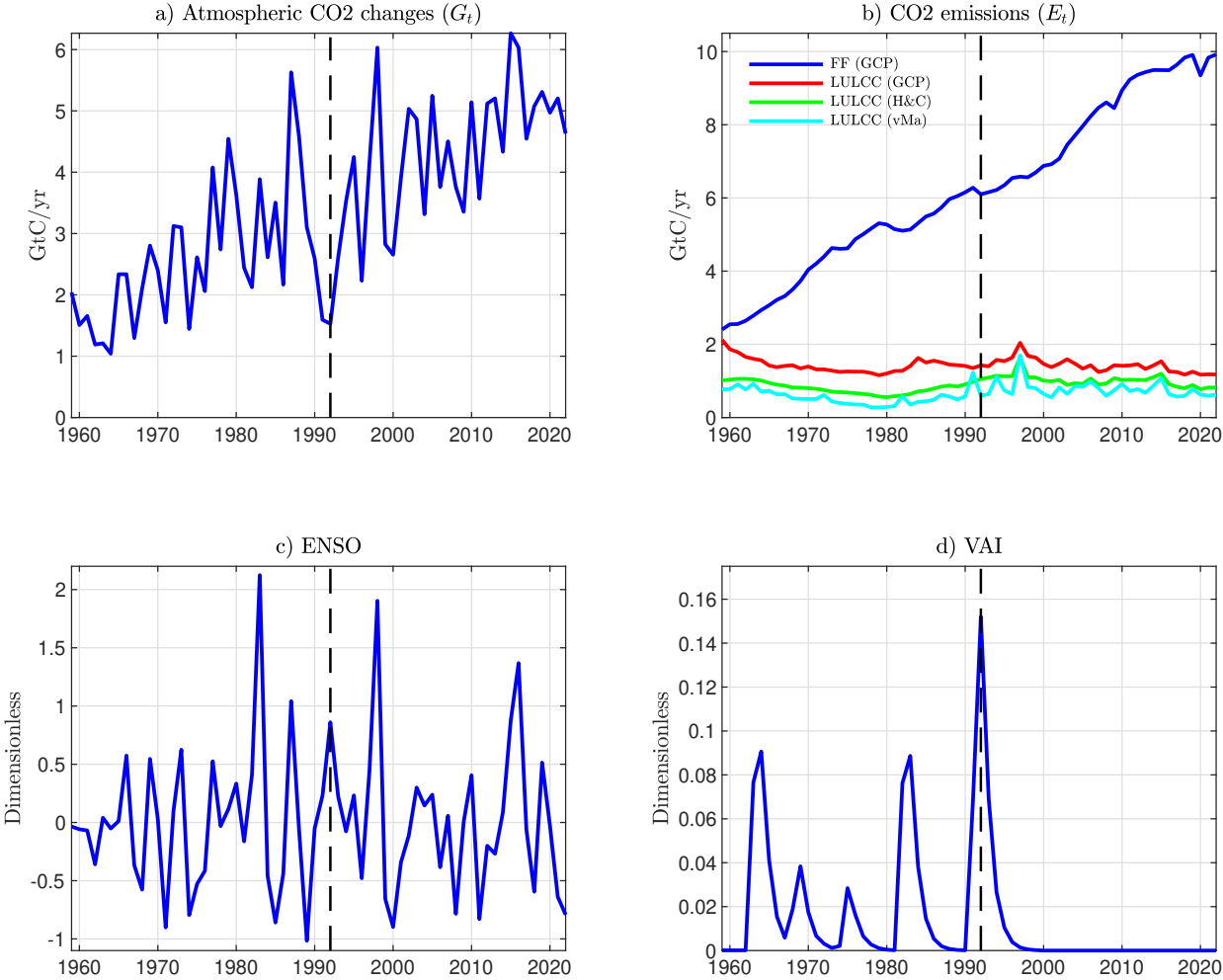


Table S2: *Least-squares regression output of the linear models in Equations (1)–(4) for the period 1959–2022 for the three data sets GCP, H&C, and vMa. “ $\hat{\alpha}$ ” denotes the estimate of the AF α , “SE($\hat{\alpha}$)” denotes the standard error of $\hat{\alpha}$, and “Relative SE” denotes the ratio of the standard error to the standard error from $\hat{\alpha}_1$, corresponding to the leftmost column. “CI_{95%}(α)” denotes a 95% confidence interval for the AF α , based on the Gaussian distribution. “ $\widehat{SD}(u_t)$ ” denotes the estimated standard deviation of the error term u_t and R^2 is the coefficient of determination. “ $\hat{\gamma}_i$ ”, $i = 1, 2$, denotes the estimates of the γ_i parameter from Equations (3)–(4) and “SD($\hat{\gamma}_i$)” is their estimated standard deviation.*

Data: GCP	(1)	(2)	(3)	(4)
$\hat{\alpha}$	0.4386	0.4478	0.4716	0.4697
SE($\hat{\alpha}$)	0.0159	0.0141	0.0126	0.0105
Relative SE	1.0000	0.8895	0.7904	0.6630
CI _{95%} (α)	[0.4074, 0.4697]	[0.4201, 0.4755]	[0.4470, 0.4962]	[0.4490, 0.4903]
$\widehat{SD}(u_t)$	0.1258	0.9088	0.0881	0.6292
R^2	0	0.5863	0.5258	0.8080
$\hat{\gamma}_1$ (ENSO)	-	-	0.1365	1.0025
SD($\hat{\gamma}_1$)	-	-	0.0168	0.1141
$\hat{\gamma}_2$ (VAI)	-	-	-2.2676	-15.1482
SD($\hat{\gamma}_2$)	-	-	0.2935	2.3688
Data: H&C	(1)	(2)	(3)	(4)
$\hat{\alpha}$	0.4763	0.4755	0.5102	0.4960
SE($\hat{\alpha}$)	0.0171	0.0151	0.0144	0.0117
Relative SE	1.0000	0.8800	0.8394	0.6814
CI _{95%} (α)	[0.4427, 0.5099]	0.4460, 0.5051]	[0.4820, 0.5384]	[0.4731, 0.5189]
$\widehat{SD}(u_t)$	0.1371	0.9148	0.0988	0.6648
R^2	0	0.5807	0.4975	0.7856
$\hat{\gamma}_1$ (ENSO)	-	-	0.1468	0.9851
SD($\hat{\gamma}_1$)	-	-	0.0205	0.1279
$\hat{\gamma}_2$ (VAI)	-	-	-2.3289	-13.6909
SD($\hat{\gamma}_2$)	-	-	0.3987	3.2461
Data: vMa	(1)	(2)	(3)	(4)
$\hat{\alpha}$	0.4957	0.4902	0.5298	0.5096
SE($\hat{\alpha}$)	0.0180	0.0155	0.0158	0.0124
Relative SE	1.0000	0.8628	0.8822	0.6935
CI _{95%} (α)	[0.4605, 0.5309]	[0.4599, 0.5206]	[0.4988, 0.5609]	[0.4852, 0.5340]
$\widehat{SD}(u_t)$	0.1431	0.9155	0.1059	0.6872
R^2	0	0.5801	0.4704	0.7709
$\hat{\gamma}_1$ (ENSO)	-	-	0.1496	0.9564
SD($\hat{\gamma}_1$)	-	-	0.0220	0.1328
$\hat{\gamma}_2$ (VAI)	-	-	-2.3440	-12.9004
SD($\hat{\gamma}_2$)	-	-	0.4594	3.5267

Table S3: *Least-squares regression output of the linear models in Equations (1)–(4) for the period 1992–2022 for the three data sets GCP, H&C, and vMa. “ $\hat{\alpha}$ ” denotes the estimate of the AF α , “SE($\hat{\alpha}$)” denotes the standard error of $\hat{\alpha}$, and “Relative SE” denotes the ratio of the standard error to the standard error from $\hat{\alpha}_1$, corresponding to the leftmost column. “ $CI_{95\%}(\alpha)$ ” denotes a 95% confidence interval for the AF α , based on the Gaussian distribution. “ $\widehat{SD}(u_t)$ ” denotes the estimated standard deviation of the error term u_t and R^2 is the coefficient of determination. “ $\hat{\gamma}_i$ ”, $i = 1, 2$, denotes the estimates of the γ_i parameter from Equations (3)–(4) and “SD($\hat{\gamma}_i$)” is their estimated standard deviation.*

Data: GCP	(1)	(2)	(3)	(4)
$\hat{\alpha}$	0.4456	0.4497	0.4626	0.4613
SE($\hat{\alpha}$)	0.0190	0.0157	0.0124	0.0104
Relative SE	1.0000	0.8247	0.6509	0.5464
$CI_{95\%}(\alpha)$	[0.4083, 0.4828]	[0.4190, 0.4804]	[0.4384, 0.4869]	[0.4409, 0.4816]
$\widehat{SD}(u_t)$	0.1065	0.9309	0.0662	0.5891
R^2	0	0.3558	0.6391	0.7592
$\hat{\gamma}_1$ (ENSO)	-	-	0.1122	1.0221
SD($\hat{\gamma}_1$)	-	-	0.0166	0.1186
$\hat{\gamma}_2$ (VAI)	-	-	-2.2281	-17.5878
SD($\hat{\gamma}_2$)	-	-	0.1702	1.2190
Data: H&C	(1)	(2)	(3)	(4)
$\hat{\alpha}$	0.4662	0.4691	0.4841	0.4811
SE($\hat{\alpha}$)	0.0203	0.0163	0.0136	0.0111
Relative SE	1.0000	0.8041	0.6678	0.5478
$CI_{95\%}(\alpha)$	[0.4264, 0.5060]	[0.4371, 0.5011]	[0.4575, 0.5107]	[0.4593, 0.5029]
$\widehat{SD}(u_t)$	0.1132	0.9346	0.0706	0.5921
R^2	0	0.3506	0.6372	0.7567
$\hat{\gamma}_1$ (ENSO)	-	-	0.1203	1.0333
SD($\hat{\gamma}_1$)	-	-	0.0191	0.1238
$\hat{\gamma}_2$ (VAI)	-	-	-2.3345	-17.4042
SD($\hat{\gamma}_2$)	-	-	0.2018	1.3348
Data: vMa	(1)	(2)	(3)	(4)
$\hat{\alpha}$	0.4786	0.4815	0.4961	0.4924
SE($\hat{\alpha}$)	0.0203	0.0159	0.0141	0.0113
Relative SE	1.0000	0.7865	0.6962	0.5598
$CI_{95\%}(\alpha)$	[0.4389, 0.5183]	[0.4503, 0.5128]	[0.4685, 0.5238]	[0.4702, 0.5146]
$\widehat{SD}(u_t)$	0.1146	0.9109	0.0732	0.5914
R^2	0	0.3832	0.6198	0.7573
$\hat{\gamma}_1$ (ENSO)	-	-	0.1213	1.0060
SD($\hat{\gamma}_1$)	-	-	0.0207	0.1272
$\hat{\gamma}_2$ (VAI)	-	-	-2.2999	-16.1863
SD($\hat{\gamma}_2$)	-	-	0.2268	1.3944

Table S4: Deming regression estimates (S2.2) of the AF α in (S2.1) for the three data sets GCP, H&C, and vMa, for the full sample 1959–2022 (left panel) and the recent sample 1992–2022 (right panel). The parameter δ denotes the measurement error ratio δ , see Section S2.5 for details.

Data	Full sample (1959-2022)					Recent sample (1992-2022)				
	$\delta = 0.2$	$\delta = 0.5$	$\delta = 1$	$\delta = 2$	$\delta = 5$	$\delta = 0.2$	$\delta = 0.5$	$\delta = 1$	$\delta = 2$	$\delta = 5$
GCP	0.4623	0.4561	0.4526	0.4504	0.4489	0.4598	0.4555	0.4531	0.4515	0.4504
H&C	0.4921	0.4852	0.4813	0.4787	0.4769	0.4802	0.4756	0.4729	0.4712	0.4700
vMa	0.5078	0.5007	0.4964	0.4936	0.4917	0.4926	0.4881	0.4854	0.4836	0.4824

Figure S3: Cumulative airborne fraction (S3.2) calculated from SSP1-2.6 data over the period 2023–2100. a) $w = 78$, corresponding to the CAF in (S3.1); b) $w = 50$; c) $w = 20$; d) $w = 10$; e) $w = 5$; f) $w = 1$, corresponding to the AF ratio-based estimator, denoted by $\hat{\alpha}_{1,t}$ in the main paper. See Section S3 for details.

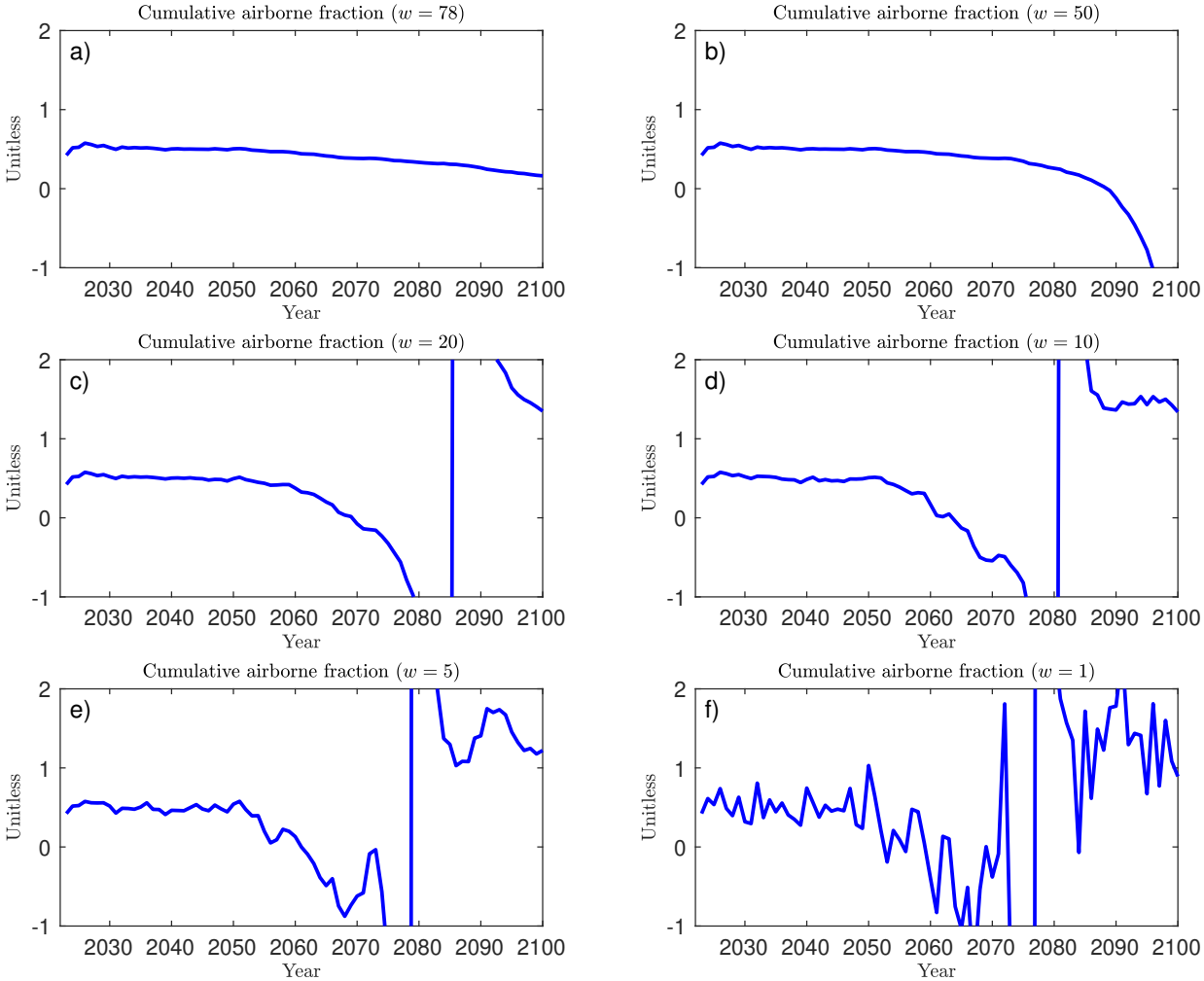


Figure S4: Simulation study of the properties of the estimators $\hat{\alpha}_1$ and $\hat{\alpha}_2$. See Section S4 for

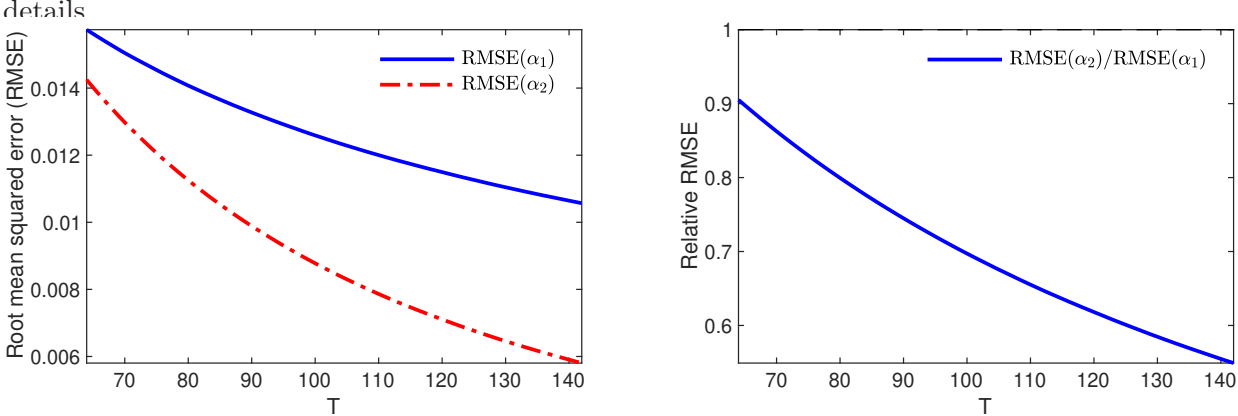


Figure S5: Analysis of SSP1-1.9 data over the period 2023–2100. a) Atmospheric concentration changes (G_t) for the historical period 1959–2022 (black) and the SSP period 2022–2100. b) Emissions (E_t) data. Magenta lines denote the original output data from MAGICC and the blue lines denote the perturbed data. c) Ratio of atmospheric changes to emissions (G_t/E_t). Black lines denote data from the Global Carbon Project over the historical period 1959–2022. Magenta lines denote the original SSP output data from MAGICC over the period 2023–2100. Blue lines denote the perturbed SSP data. The red line in c) is the regression-based estimator $\hat{\alpha}_{2,t} = \hat{\mathbb{E}}(\alpha_t | \text{data})$ of the time-varying airborne fraction α_t , obtained from the Kalman smoother. Shaded area is a 95% confidence band around $\hat{\alpha}_{2,t}$.

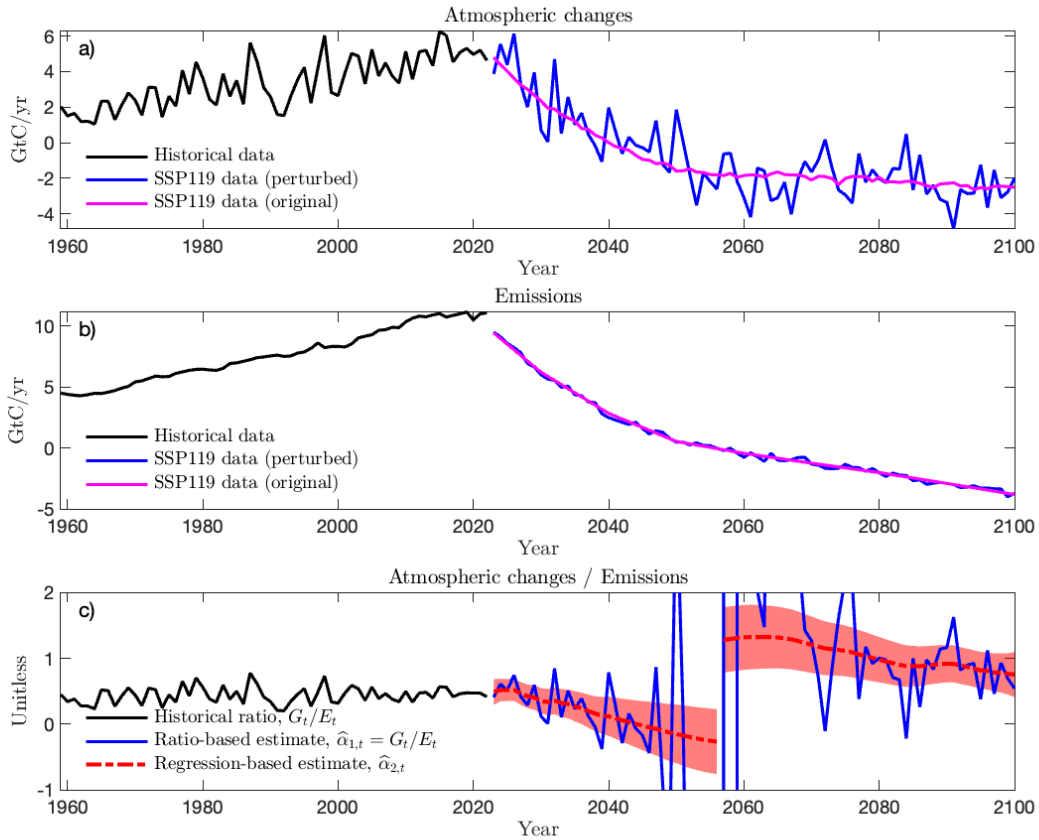


Figure S6: Analysis of SSP2-4.5 data over the period 2023–2100. a) Atmospheric concentration changes (G_t) for the historical period 1959–2022 (black) and the SSP period 2022–2100. b) Emissions (E_t) data. Magenta lines denote the original output data from MAGICC and the blue lines denote the perturbed data. c) Ratio of atmospheric changes to emissions (G_t/E_t). Black lines denote data from the Global Carbon Project over the historical period 1959–2022. Magenta lines denote the original SSP output data from MAGICC over the period 2023–2100. Blue lines denote the perturbed SSP data. The red line in c) is the regression-based estimator $\hat{\alpha}_{2,t} = \hat{\mathbb{E}}(\alpha_t | \text{data})$ of the time-varying airborne fraction α_t , obtained from the Kalman smoother. Shaded area is a 95% confidence band around $\hat{\alpha}_{2,t}$.

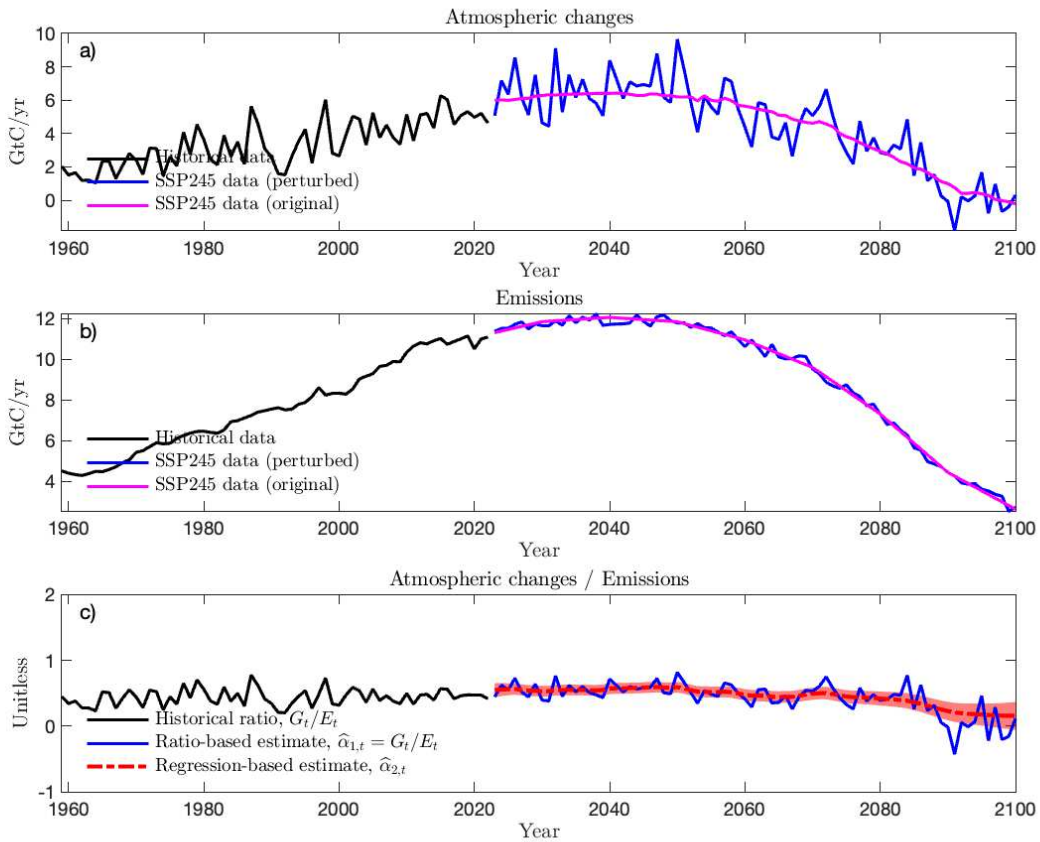


Figure S7: Analysis of SSP3-7.0 data over the period 2023–2100. a) Atmospheric concentration changes (G_t) for the historical period 1959–2022 (black) and the SSP period 2022–2100. b) Emissions (E_t) data. Magenta lines denote the original output data from MAGICC and the blue lines denote the perturbed data. c) Ratio of atmospheric changes to emissions (G_t/E_t). Black lines denote data from the Global Carbon Project over the historical period 1959–2022. Magenta lines denote the original SSP output data from MAGICC over the period 2023–2100. Blue lines denote the perturbed SSP data. The red line in c) is the regression-based estimator $\hat{\alpha}_{2,t} = \hat{\mathbb{E}}(\alpha_t | \text{data})$ of the time-varying airborne fraction α_t , obtained from the Kalman smoother. Shaded area is a 95% confidence band around $\hat{\alpha}_{2,t}$.

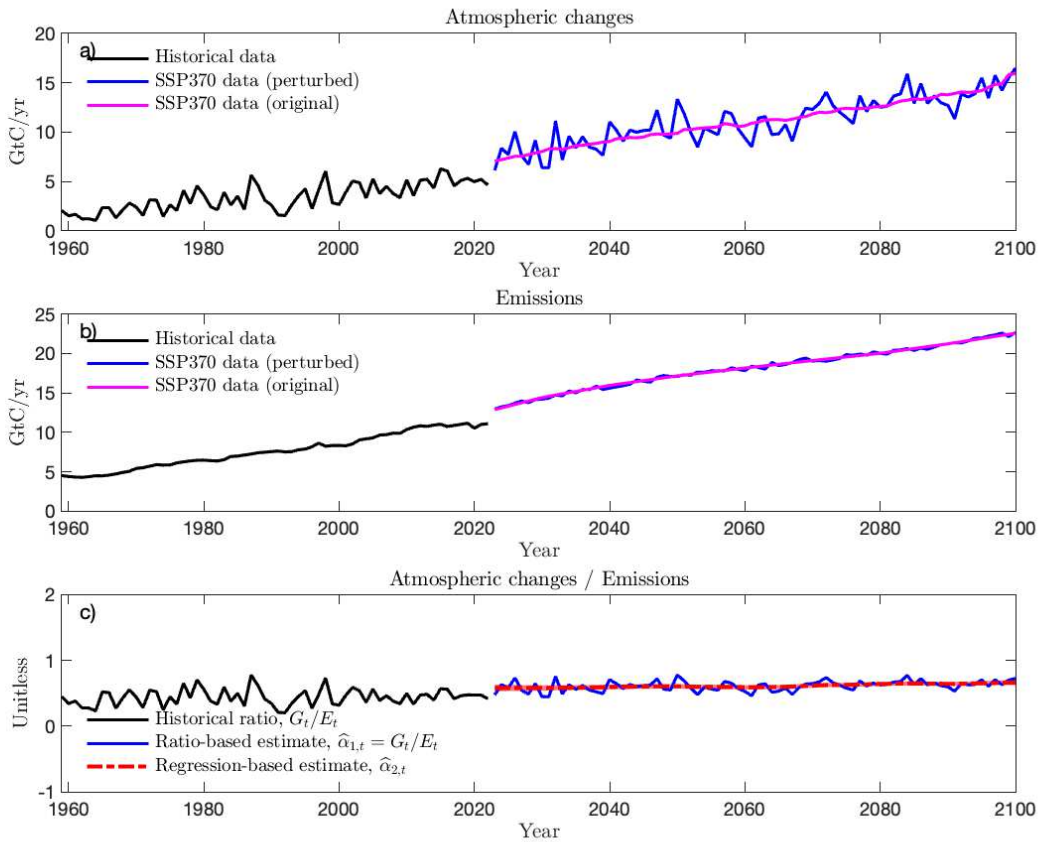


Figure S8: Analysis of SSP4-3.4 data over the period 2023–2100. a) Atmospheric concentration changes (G_t) for the historical period 1959–2022 (black) and the SSP period 2022–2100. b) Emissions (E_t) data. Magenta lines denote the original output data from MAGICC and the blue lines denote the perturbed data. c) Ratio of atmospheric changes to emissions (G_t/E_t). Black lines denote data from the Global Carbon Project over the historical period 1959–2022. Magenta lines denote the original SSP output data from MAGICC over the period 2023–2100. Blue lines denote the perturbed SSP data. The red line in c) is the regression-based estimator $\hat{\alpha}_{2,t} = \hat{\mathbb{E}}(\alpha_t | \text{data})$ of the time-varying airborne fraction α_t , obtained from the Kalman smoother. Shaded area is a 95% confidence band around $\hat{\alpha}_{2,t}$.

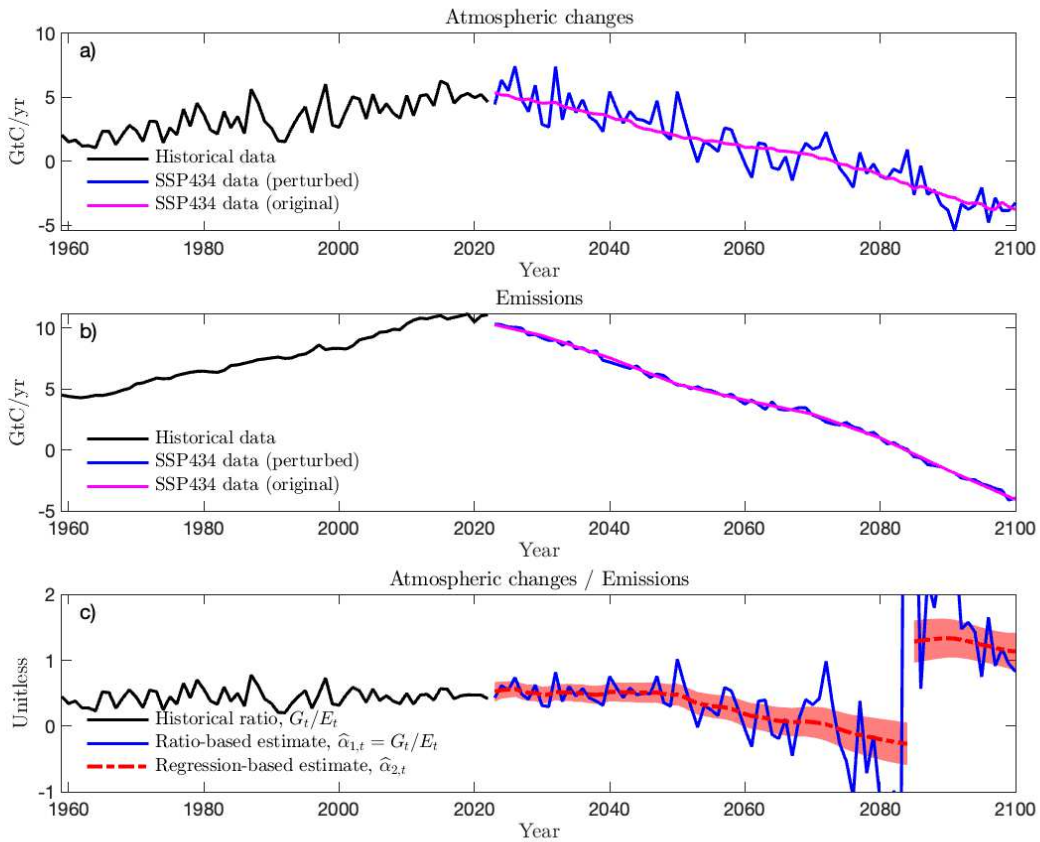


Figure S9: Analysis of SSP5-8.5 data over the period 2023–2100. a) Atmospheric concentration changes (G_t) for the historical period 1959–2022 (black) and the SSP period 2022–2100. b) Emissions (E_t) data. Magenta lines denote the original output data from MAGICC and the blue lines denote the perturbed data. c) Ratio of atmospheric changes to emissions (G_t/E_t). Black lines denote data from the Global Carbon Project over the historical period 1959–2022. Magenta lines denote the original SSP output data from MAGICC over the period 2023–2100. Blue lines denote the perturbed SSP data. The red line in c) is the regression-based estimator $\hat{\alpha}_{2,t} = \hat{\mathbb{E}}(\alpha_t | \text{data})$ of the time-varying airborne fraction α_t , obtained from the Kalman smoother. Shaded area is a 95% confidence band around $\hat{\alpha}_{2,t}$.

